AIMS Mathematics, 11(1): 511–542.
DOI: 10.3934/math.2026022
Received: 15 November 2025
Revised: 25 December 2025
Accepted: 29 December 2025
Published: 07 January 2026

https://www.aimspress.com/journal/Math

Research article

The bimodal two-piece skew-normal distribution: Mathematical theory, reliability aging measures, and simulation-oriented decision analysis

Reda Elbarougy[1], Jondeep Das[2], Partha Jyoti Hazarika[3] and Mohamed S. Eliwa[4,*]

[1] Department of Artificial Intelligence and Data Science, College of Computer Science and Engineering, University of Ha'il, Saudi Arabia
[2] Department of Statistics, Bhattadev University, Bajali, Assam, India
[3] Department of Statistics, Dibrugarh University, Dibrugarh, Assam, India
[4] Department of Statistics and Operations Research, College of Science, Qassim University, Saudi Arabia

* **Correspondence:** Email: m.eliwa@qu.edu.sa.

Abstract: This study introduces a novel and adaptable bimodal class of two-piece skew-normal distributions, specifically designed to accommodate datasets with up to two modes. This paper comprehensively examines the analytical attributes of the suggested model, encompassing its cumulative distribution function, moments, moment generating function, Rényi entropy, reliability metrics with aging intensity, and other critical statistical properties. The model effectively captures asymmetric behavior, accommodating both negative and positive skewness, and is particularly well suited for leptokurtic data characterized by an increasing hazard rate. Furthermore, it adeptly manages both over- and under-dispersed data, enhancing its relevance across many domains. To improve its adaptability, extensions of the distribution concerning location and scale are also devised. Parameter estimation is conducted using the maximum likelihood approach. A detailed simulation study assesses the performance of the estimators, illustrating their asymptotic consistency and efficiency. The practical utility of the suggested distribution is demonstrated through applications to real-world datasets, where it regularly outperforms multiple existing rival models in goodness-of-fit. Finally, a likelihood ratio test is utilized to statistically validate the superiority of the presented model compared to its nested alternatives.

Keywords: statistical model; bimodal data modeling; non-symmetric and leptokurtic distributions; failure analysis; simulation; likelihood ratio test; decision-making
Mathematics Subject Classification: 60E05, 62E15, 62F10, 62N05, 62P99

1. Introduction

Statistics and the applied sciences have long relied on the normal (N) distribution as a fundamental probability model due to its mathematical tractability and its frequent emergence in real-world phenomena; see [1, 2]. It underpins a wide range of methodologies, including regression modeling, measurement error theory, and classical statistical inference. Nevertheless, in fields such as reliability analysis, environmental sciences, economics, and biology, empirical data often display skewness or asymmetry. Because the N distribution is inherently symmetric, it is generally inadequate for modeling such asymmetric data structures. In 1985, Azzalini and colleagues expanded the N model with the skew-normal (SN) distribution, which has a shape parameter that adjusts the degree and direction of skewness, in order to circumvent this constraint [3]. There is a probability density function (PDF) for the SN distribution that is given by

$$f(x;\lambda) = 2\phi(x)\Phi(\lambda x), \qquad x \in \mathbb{R}, \lambda \in \mathbb{R}, \tag{1.1}$$

where $\phi(\cdot)$ represents the standard N distribution's PDF, and $\Phi(\cdot)$ stands for its cumulative distribution function (CDF). The asymmetry parameter, which controls the distribution's asymmetry, is another name for the additional parameter $\lambda(\in \mathbf{R})$. Modern statistical modeling relies heavily on the SN distribution, which has been extensively expanded since its inception to account for more nuanced properties, including bimodality, kurtosis fluctuations, and thicker tails. Many skewed families have been suggested since the SN distribution was introduced, as previously mentioned. The skewed distribution families proposed in [4, 5] are particularly noteworthy. For further details, see [6, 7]. These models extend the classical framework by incorporating additional parameters that allow greater flexibility in controlling skewness. Improving the flexibility of skewed model creation, [8] introduced a new skew-logistic distribution that uses an innovative skew technique independent of a CDF. The tanh-SN distribution, which incorporates the hyperbolic tangent function, was developed by Mahmoud [9] as a more modern and significant variation of the SN distribution. A smooth and flexible type of skewness can be achieved using the distribution while maintaining analytical tractability, thanks to the hyperbolic tangent function. Although these models are quite flexible for asymmetric data, most of them are made for unimodal distributions. In fact, however, many datasets in the real world have bimodal or even multimodal features. There is a great deal of literature on this kind of data, such as studies on metabolic rates [10], chemical and physical mixtures [11], precipitation and rainfall data [12], hydrological measurements [13], environmental processes [14], and social or biological phenomena [15, 16]. These examples show how important it is to build probability models that can handle multimodal behavior in data. Recent research has focused on creating adaptable families of distributions capable of modeling data with several modes. [17] introduced a category of symmetric and asymmetric bimodal distributions by incorporating additional parameters into the Azzalini SN model. In their study, they introduced an innovative two-parameter bimodal skew-normal (BSN) distribution defined by the subsequent PDF as

$$f(x;\alpha,\lambda) = 2\,\frac{1+\alpha x^2}{1+\alpha}\,\phi(x)\,\Phi(\lambda x), \qquad x \in \mathbb{R},\ \lambda \in \mathbb{R},\ \alpha \geq 0, \tag{1.2}$$

which effectively represents data-sets that exhibit two separate modes. In a similar vein, [18] introduces the bimodal tanh-skew-normal distribution, which extends the tanh-skew-normal distribution presented

by [9]. Alongside the BSN distribution, various other families have been created to represent bimodality and asymmetry through various methodologies. The list comprises the alpha-SN (ASN) distribution introduced by [19], the alpha-SL distribution by [20,21], the generalized ASN distribution by [22], and the generalized ASL distribution by [23]. The PDF of the ASN distribution as shown in [19] is expressed as

$$f(x;\alpha) = \frac{(1-\alpha x)^2+1}{2+\alpha^2}\,\phi(x), \qquad x \in \mathbb{R},\ \alpha \in \mathbb{R}. \tag{1.3}$$

Additional significant advancements encompass the Balakrishnan ASN distribution [24], the Balakrishnan ASL distribution [25,26], and the Balakrishnan log ASN distribution [27]. Additionally, the bimodal skew-symmetric normal distribution proposed by [21] constitutes a significant advancement in the examination of asymmetric bimodal models. Besides, [28, 29] also reflect some significant results regarding the multimodality of some asymmetric normal distributions. In addition, recent advancements in degradation modeling have emphasized robust Bayesian frameworks for online state estimation under outliers and parameter uncertainty [30], as well as conjugate-prior-based inference and online model prediction for homogeneous and heterogeneous Gamma process models [31], further highlighting the growing interest in flexible and computationally efficient reliability modeling approaches.

The two-piece normal (TPN) distribution was proposed by [32] as a versatile family of uni- and bimodal distributions that extends the conventional normal model to accommodate asymmetry while maintaining analytical manageability. This model partitions the real line into two parts, each characterized by a normal distribution with varying scale parameters, thus facilitating divergent behavior on either side of the mode. Formally, if a random variable X adheres to a TPN distribution characterized by the shape parameter λ, represented as $X \sim TPN(\lambda)$, its PDF is articulated as

$$g(x;\lambda) = \phi(x)\, e^{-\lambda^2/2} \cosh(\lambda x), \qquad x \in \mathbb{R},\ \lambda \geq 0, \tag{1.4}$$

where $\phi(x)$ signifies the ordinary normal probability density function and $\cosh(\cdot)$ denotes the hyperbolic cosine function. The TPN distribution preserves the essential traits of the normal distribution, including smoothness and unimodality, while incorporating an additional parameter λ that regulates skewness and tail features. Depending on the value of λ, the model can generate symmetric, moderately skewed, or heavy-tailed distributions, thus providing a compromise between interpretability and flexibility. Due to these characteristics, the TPN distribution acts as a foundational baseline for developing more broad asymmetric or bimodal distribution families. Recent developments in bimodal and asymmetric modeling have introduced several flexible extensions of the skew-normal and related distributions. However, many of these models still exhibit important limitations when applied to real-world data. First, most existing bimodal families, such as the BSN, ASN, and Balakrishnan-type variants, allow skewness control but do not provide independent regulation of skewness and bimodality, which restricts their ability to flexibly tune the prominence and separation of the two modes. Second, several bimodal transformations rely on complex stochastic constructions or nonlinear perturbations that hinder analytical tractability, making it difficult to derive closed-form expressions for moments, entropy, or reliability measures. Third, many classical bimodal extensions are limited in capturing diverse hazard-rate shapes, which reduces their applicability in survival or reliability modeling. Furthermore, in some cases, parameter estimation becomes unstable due to strong dependence between

shape parameters or irregular likelihood surfaces. To address these limitations, this study enhances the TPN distribution from [32] by incorporating an extra shape parameter to simultaneously account for skewness and bimodality. This construction enables independent control of skewness and bimodality, provides closed-form expressions for several key statistical and reliability properties, and supports a wide range of hazard-rate behaviours. As demonstrated in later sections, the proposed model offers both theoretical tractability and superior practical flexibility compared with existing bimodal models. This new distribution is developed based on the ASN distribution outlined in [19]. Additionally, real-life applications are performed to assess the efficacy of the new distribution in conjunction with simulation studies.

The subsequent sections of this article are structured as follows. Section 2 presents the newly proposed bimodal expansion of the TPN distribution. This section also includes graphical representations to illustrate the impact of the shape parameters on the distribution's structure and dynamics. Section 3 delineates critical structural aspects of the NTPN distribution, encompassing its cumulative distribution function, moment generating function, raw moments, mean deviation, mode, Rényi entropy, and reliability qualities, thus providing a thorough theoretical framework. Section 4 elaborates on the location and scale extensions of the NTPN model, subsequently presenting the formulation of maximum likelihood estimation (MLE) processes. Section 5 presents a comprehensive simulation analysis to evaluate the performance and consistency of the maximum likelihood estimators across diverse parameter configurations and sample sizes. Section 6 presents empirical data applications to assess the practical applicability and goodness-of-fit of the suggested distribution relative to other models. Section 7 is accountable for the outcome of the likelihood ratio test. Section 8 finishes the article by summarizing the principal findings, theoretical implications, and prospective avenues for further research.

2. Mathematical framework and visualization: NTPN model

A continuous random variable X is said to adhere to the NTPN distribution if its PDF is specified as

$$f(x;\alpha,\lambda) = \frac{(1-\alpha x)^2+1}{C(\alpha,\lambda)} g(x;\lambda), \quad x \in \mathbb{R}, \lambda \geq 0, \alpha \in \mathbb{R}, \tag{2.1}$$

where $g(x;\lambda)$ denotes the PDF of the TPN distribution as specified in Eq (1.4) and $C(\alpha,\lambda)$ denotes the normalizing constant, where

$$C(\alpha,\lambda) = \int_{-\infty}^{\infty} \left((1-\alpha x)^2+1\right) g(x;\lambda)\, dx = \alpha^2\left(\lambda^2+1\right)+2.$$

For simplicity, $C(\alpha,\lambda)$ is denoted by C. The new distribution is referred to as $NTPN(\alpha,\lambda)$ or simply the NTPN distribution. The graphical presentation of the PDF of NTPN distribution is depicted in Figure 1 for different values of the parameters.

From Figure 1(a), it can be observed that with λ fixed at 1.38 and α varying 1.52 to 3.52, the distribution exhibits a distinct bimodal structure. Increasing α results in a noticeable shift of the right-hand peak toward higher x-values, accompanied by a reduction in its height. This indicates that α primarily influences the skewness and the relative prominence of the two peaks. Again, Figure 1(b) shows that for a fixed $\alpha = 1.25$ and varying λ from 0.24 to 0.95, the bimodal structure is preserved,

but changes in λ alter the height and separation of the peaks. Larger λ values reduce the height of the left-hand peak while slightly shifting the density mass toward the right. This suggests that λ regulates the spread and balance of the two modes. Again, from Figure 1(c) it can be established that if both the two parameters are considered to be zero, then the NTPN distribution reduces to a normal distribution (with a unimodal symmetric shape). Again, when λ is considered to be zero, the NTPN distribution reduces to an ASN distribution of [19]. Similarly, from Figure 1(d) it can be observed that the NTPN distribution reduces to a TPN distribution of [32] when α is considered to be zero.

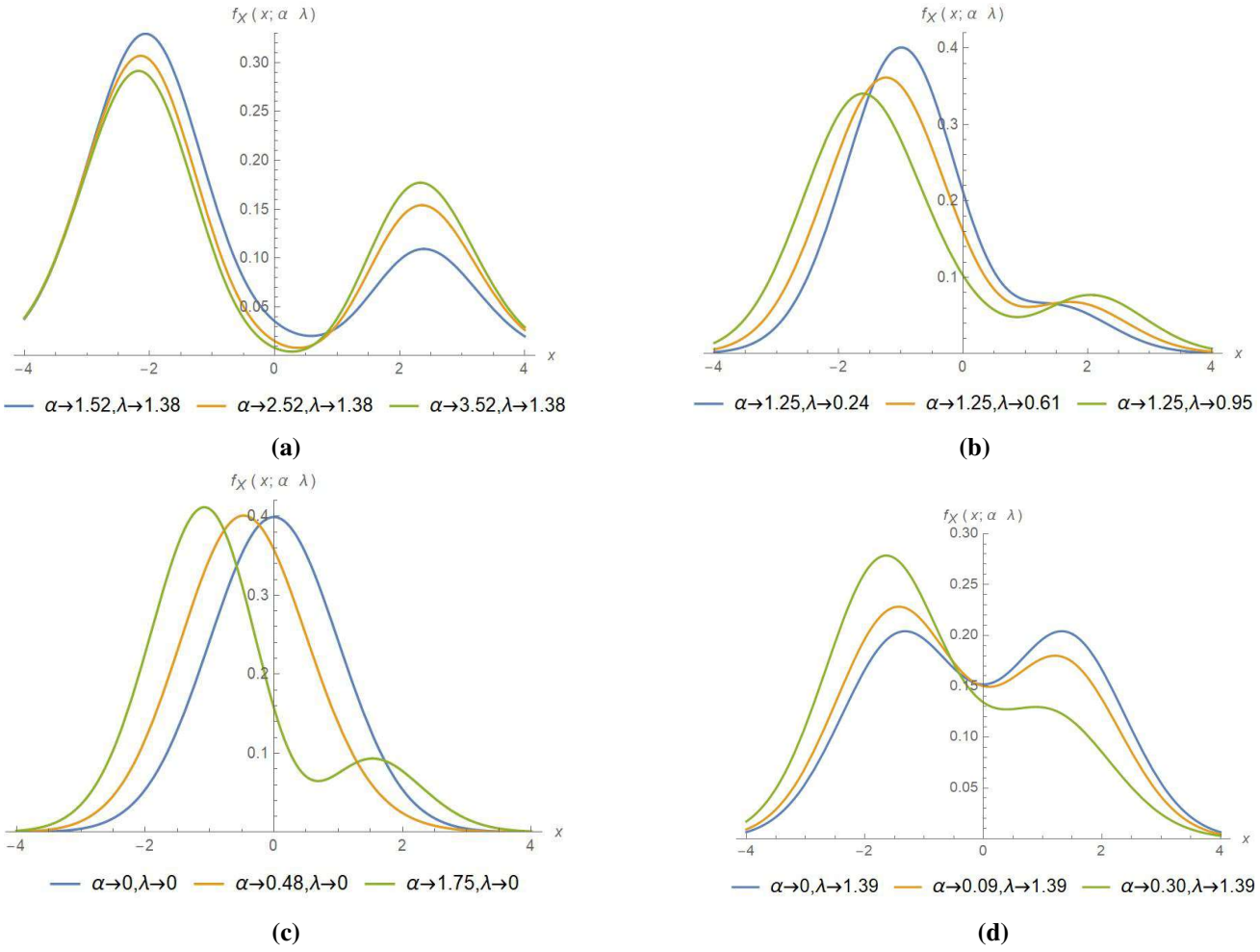

Figure 1. The PDF of the NTPN distribution.

The parameter-dependent properties examined here emphasize the interpretability and flexibility of the NTPN distribution and reveal its structural connections with previously studied asymmetric and bimodal distributional families. The functional form of the NTPN density satisfies the identity,

$$(1 + \alpha x)^2 = (1 - \alpha(-x))^2,$$

which directly implies

$$f(x; -\alpha, \lambda) = f(-x; \alpha, \lambda).$$

Integrating both sides with respect to x yields the following relationship between the corresponding CDF:

$$F(x; -\alpha, \lambda) = 1 - F(-x; \alpha, \lambda). \tag{2.2}$$

Equation (2.2) shows that reversing the sign of the skewness parameter α produces a mirror-image distribution about the origin. Consequently, the parameter α governs the direction of skewness in a manner consistent with other skewed distributional families, such as the ASN and BSN models. Moreover, the proposed NTPN distribution encompasses several prominent models as special or limiting cases. Specifically,

$$F(x; 0, \lambda) = F_{\text{TPN}}(x; \lambda), \qquad F(x; \alpha, 0) = F_{\text{ASN}}(x; \alpha),$$

and

$$F(x; 0, 0) = \Phi(x),$$

where F_{TPN} denotes the cumulative distribution function of the TPN distribution [32], F_{ASN} represents the cumulative distribution function of the ASN distribution [19], and $\Phi(\cdot)$ is the standard normal cumulative distribution function. These relationships clarify the distinct roles of the model parameters: The parameter α controls directional skewness, whereas the parameter λ regulates tail behavior, multimodality, and peakedness. In particular, setting $\alpha = 0$ removes skewness, while setting $\lambda = 0$ eliminates the two-piece structure of the distribution. The CDF of the NTPN distribution is obtained by integrating its PDF given in Eq (2.1). Thus, the CDF can be expressed as

$$\begin{aligned} F(x; \alpha, \lambda) =& \frac{1}{2C}\Big[B\,\Phi(x-\lambda) + (C + 2\alpha\lambda - B)\,\Phi(x+\lambda) \\ &+ \alpha\phi(\lambda + x)\left\{e^{2\lambda x}[\alpha(\lambda + x) - 2] + \alpha(-\lambda + x + 2)\right\}\Big], \end{aligned} \tag{2.3}$$

where

$$B = \alpha^2(\lambda^2 + 1) - 2\alpha\lambda + 2.$$

Starting from the definition

$$F(x; \alpha, \lambda) = \int_{-\infty}^{x} f(t; \alpha, \lambda)\, dt = \frac{1}{C}\int_{-\infty}^{x} ((1 - \alpha t)^2 + 1)\, g(t; \lambda)\, dt,$$

the integral can be decomposed as

$$\begin{aligned} F(x; \alpha, \lambda) &= \frac{1}{C}\left[\int_{-\infty}^{x} g(t; \lambda)\, dt - 2\alpha \int_{-\infty}^{x} t\, g(t; \lambda)\, dt + \alpha^2 \int_{-\infty}^{x} t^2\, g(t; \lambda)\, dt\right] \\ &= \frac{1}{C}\Big[I_0(x) - 2\alpha I_1(x) + \alpha^2 I_2(x)\Big], \end{aligned}$$

where $I_0(x)$ represents the CDF of the TPN distribution introduced by [32], and the other terms are given by

$$I_1(x) = \int_{-\infty}^{x} t\, g(t; \lambda)\, dt = \frac{\lambda}{2}[\Phi(x - \lambda) - \Phi(x + \lambda)] + \frac{1}{2}\phi(x + \lambda)(e^{2\lambda x} + 1),$$

$$I_2(x) = \int_{-\infty}^{x} t^2\, g(t;\lambda)\, dt = \frac{1}{2}(\lambda^2+1)[\Phi(x-\lambda)+\Phi(x+\lambda)-1] + \frac{1}{2}\phi(x+\lambda)[\lambda - e^{2\lambda x}(\lambda+x)-x] + \frac{1}{2}(\lambda^2+1).$$

Substituting these expressions into the above equation yields the closed-form CDF given in Eq (2.3). The CDF of the NTPN distribution for different parameter combinations of α and λ is illustrated in Figure 2. Figure 2(a) displays the CDF for fixed $\alpha = 0.1$ and varying λ values, showing how the scale parameter λ influences the steepness and spread of the curve. Figure 2(b) demonstrates the combined effects of α and λ, revealing that α primarily controls the skewness and tail behavior of the distribution, while λ governs its location and dispersion. Overall, these plots highlight the flexibility of the NTPN distribution in modeling both symmetric and asymmetric data structures.

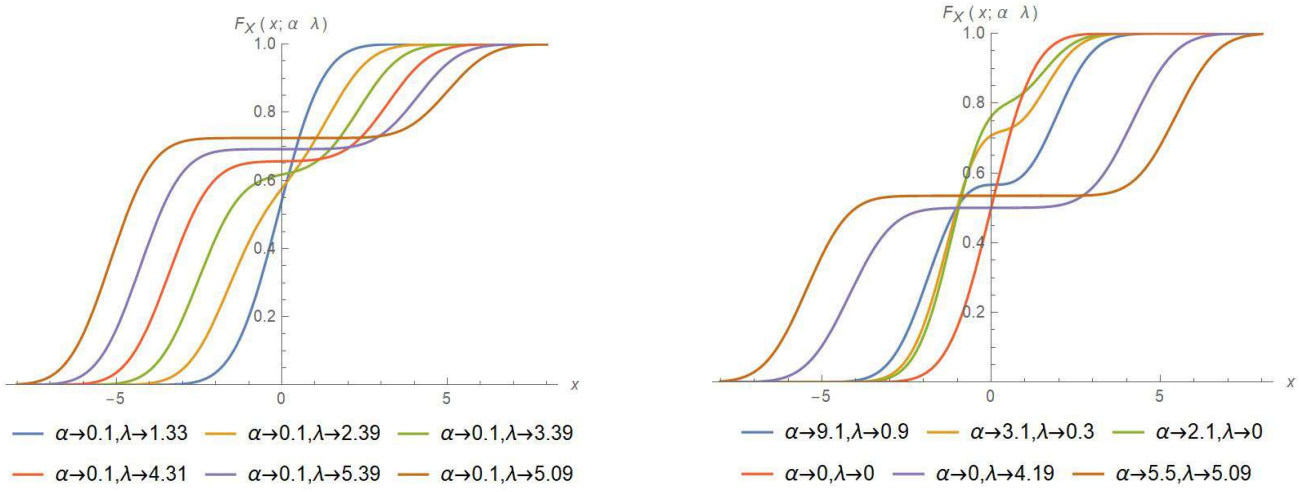

(a) **(b)**

Figure 2. The CDF of the NTPN distribution.

3. Statistical and reliability properties

3.1. Capability to exhibit two modes

To investigate the modality of the NTPN distribution, we analyze the critical points of the density function $f(x;\alpha,\lambda)$ given in Eq (2.1). Differentiating the density with respect to x yields

$$f'(x;\alpha,\lambda) = \frac{e^{-\frac{1}{2}(\lambda^2+x^2)}}{\sqrt{2\pi}\,C}\Big[A(x)\,\sinh(\lambda x) - B(x)\,\cosh(\lambda x)\Big], \tag{3.1}$$

where $A(x) = \lambda(\alpha^2x^2 - 2\alpha x + 2)$, and $B(x) = 2\alpha + \alpha^2x^3 - 2\alpha x^2 - 2(\alpha^2-1)x$. Since $\cosh(\lambda x) > 0$ for all $x \in \mathbb{R}$ and $\sinh(\lambda x)$ is strictly increasing on $\mathbb{R}$, the zeros of $f'(x;\alpha,\lambda)$ are exactly the solutions of

$$H(x) = A(x)\,\tanh(\lambda x) - B(x) = 0. \tag{3.2}$$

Again, the function $\tanh(\lambda x)$ is strictly increasing and bounded between -1 and 1. Besides, $A(x)$ is a quadratic polynomial, and $B(x)$ is a cubic polynomial. Thus, $A(x)\tanh(\lambda x)$ is the product of

a quadratic polynomial and a smooth monotone function, and $B(x)$ is a smooth cubic polynomial. Hence, $H(x)$ is a smooth function on $\mathbb{R}$, whose curvature is governed by at most cubic behavior. Differentiating $H(x)$ gives

$$H'(x) = A'(x)\tanh(\lambda x) + A(x)\lambda\,\mathrm{sech}^2(\lambda x) - B'(x),$$

where

$$A'(x) \text{ is linear}, \qquad B'(x) \text{ is quadratic}, \qquad \mathrm{sech}^2(\lambda x) \text{ is strictly decreasing for } x > 0.$$

Thus, $H'(x)$ is the sum of at most quadratic polynomial terms and monotone, bounded functions, which implies that $H'(x)$ can change sign at most twice. Hence, $H(x)$ can have at most three real zeros. Each zero of $H(x)$ corresponds to a critical point of $f(x;\alpha,\lambda)$. A smooth density f may have at most as many local extrema as the number of distinct real zeros of f'. Since $f'(x;\alpha,\lambda)$ has at most three real zeros, the density $f(x;\alpha,\lambda)$ can exhibit at most two local maxima. Therefore, the NTPN distribution can have at most two modes.

3.2. Analysis of moments and key descriptive features: Theoretical and computational perspectives

Theorem 3.1. *The r^{th} order moment of the NTPN distribution is*

$$E(X^r) = \frac{((-1)^r - 1)\, e^{-\frac{\lambda^2}{2}} 2^{\frac{r}{2}-\frac{1}{2}}}{\sqrt{2\pi}C}\Bigg[\sqrt{2}\alpha r\Gamma\left(\frac{r}{2}\right) M\left(\frac{r}{2}+1;\frac{1}{2};\frac{\lambda^2}{2}\right) + \Gamma\left(\frac{r+1}{2}\right)\Bigg\{2M\left(\frac{r+1}{2};\frac{1}{2};\frac{\lambda^2}{2}\right) + \alpha^2(r+1)M\left(\frac{r+3}{2};\frac{1}{2};\frac{\lambda^2}{2}\right)\Bigg\}\Bigg], \tag{3.3}$$

where $M(a,b,z) = {}_1F_1(a;b;z)$ is the confluent hypergeometric function of the first kind [33].

Proof. Using the expression of the PDF given in Eq (2.1), the r^{th} order moment of the NTPN distribution is defined as:

$$\begin{aligned}
E(X^r) &= \int_{-\infty}^{\infty} x^r f(x;\alpha,\lambda)dx \\
&= \frac{1}{C}\int_{-\infty}^{\infty} x^r((1-\alpha x)^2+1)\, g(x;\lambda)\, dx \\
&= \frac{1}{C}\int_{-\infty}^{\infty} x^r\left(2 - 2\alpha x + \alpha^2 x^2\right) g(x;\lambda)\, dx \\
&= \frac{1}{C}\left[2\int_{-\infty}^{\infty} x^r g(x;\lambda)dx - 2\alpha\int_{-\infty}^{\infty} x^{r+1} g(x;\lambda)dx + \alpha^2\int_{-\infty}^{\infty} x^{r+2} g(x;\lambda)dx\right] \\
&= \frac{1}{C}\left[2I_6(x) - 2\alpha I_7(x) + \alpha^2 I_8(x)\right].
\end{aligned}$$

It can be easily understood that I_6 is the r^{th} order moment of the TPN distribution, which was calculated by [32]. Again, the remaining integrations are calculated as

$$I_7(x) = \int_{-\infty}^{\infty} x^{r+1} g(x;\lambda)dx = -\frac{2^{\frac{r}{2}-\frac{1}{2}}((-1)^r - 1)\,1}{\sqrt{\pi}}\Gamma\left(\frac{r}{2}+1\right) {}_1F_1\left(\frac{1}{2}(-r-1);\frac{1}{2};-\frac{\lambda^2}{2}\right),$$

$$I_8(x) = \int_{-\infty}^{\infty} x^{r+2} g(x;\lambda)dx = \frac{2^{\frac{r+1}{2}-\frac{1}{2}}\left((-1)^r+1\right)}{\sqrt{\pi}}\Gamma\left(\frac{r+3}{2}\right){}_1F_1\left(-\frac{r}{2}-1;\frac{1}{2};-\frac{\lambda^2}{2}\right).$$

Using these values, the final expression for moments of the NTPN distribution is evaluated and obtained as

$$E(X^r) = \frac{\left((-1)^r-1\right)e^{-\frac{\lambda^2}{2}}2^{\frac{r}{2}-\frac{1}{2}}}{\sqrt{2\pi}C}\Bigg[\sqrt{2}\alpha r\Gamma\left(\frac{r}{2}\right)M\left(\frac{r}{2}+1;\frac{1}{2};\frac{\lambda^2}{2}\right)+\Gamma\left(\frac{r+1}{2}\right)\Bigg\{2M\left(\frac{r+1}{2};\frac{1}{2};\frac{\lambda^2}{2}\right)$$
$$+\alpha^2(r+1)M\left(\frac{r+3}{2};\frac{1}{2};\frac{\lambda^2}{2}\right)\Bigg\}\Bigg].$$

□

Considering $r = 1, 2, 3, 4$ in Eq (3.3), the first four moments are calculated and obtained as

$$E(X) = -\frac{2\alpha(\lambda^2+1)}{C}, \qquad E(X^2) = \frac{\alpha^2(3A)+2(\lambda^2+1)}{C},$$
$$E(X^3) = -\frac{6\alpha A}{C}, \qquad E(X^4) = \frac{3\left[5\alpha^2 B+2A\right]}{C}.$$

Using the relationship between the raw and central moments, variance, coefficient of skewness (γ_1), and coefficient of kurtosis (γ_2) of the NTPN distribution are obtained as

$$Var(X) = \frac{(3\alpha^2A+2(\lambda^2+1))C-4\alpha^2(\lambda^2+1)^2}{C^2},$$
$$\gamma_1 = \frac{\alpha\left[-6AC^2+6(\lambda^2+1)C(3\alpha^2A+2(\lambda^2+1))-16\alpha^2(\lambda^2+1)^3\right]}{C^3\,\sigma^3},$$
$$\gamma_2 = \frac{3BC^3-48\alpha^2(\lambda^2+1)AC^2+24\alpha^2(\lambda^2+1)^2(3\alpha^2A+2(\lambda^2+1))C-48\alpha^4(\lambda^2+1)^4}{C^4\,\sigma^4},$$

where

$$A = \frac{\lambda^4}{3}+2\lambda^2+1, \qquad B = 5\alpha^2\left(\frac{\lambda^6}{15}+\lambda^4+3\lambda^2+1\right)+2\left(\frac{\lambda^4}{3}+2\lambda^2+1\right),$$
$$C = \alpha^2(\lambda^2+1)+2.$$

Table 1 displays numerical values for the mean, variance, skewness, and kurtosis coefficients of the NTPN distribution for specified values of α and λ. The results in Table 1 illustrate the considerable flexibility of the NTPN distribution in capturing diverse data behaviors. For small values of $|\alpha|$, the distribution exhibits symmetric or nearly symmetric shapes, whereas larger values of $|\alpha|$ produce strongly skewed distributions in either direction. Across all examined values, the distribution remains leptokurtic, indicating its ability to model heavy-tailed phenomena effectively. Furthermore, the analysis of the dispersion index reveals that the NTPN distribution can accommodate both under-dispersed and over-dispersed data, highlighting its practical utility in modeling a wide range of real-world datasets.

Table 1. Some descriptive computations for the NTPN model.

α	λ	Mean	Variance (σ^2)	Skewness (γ_1)	Kurtosis (γ_2)
−2.0	0.5	1.578	1.204	1.862	3.789
−1.5	0.5	1.211	1.065	1.437	3.562
−1.0	0.5	0.800	0.960	0.975	3.447
−0.5	0.5	0.397	0.933	0.486	3.221
0.5	0.5	−0.397	0.933	−0.486	3.221
1.0	0.5	−0.800	0.960	−0.975	3.447
1.5	0.5	−1.211	1.065	−1.437	3.562
2.0	0.5	−1.578	1.204	−1.862	3.789

3.3. Mean absolute deviation

Theorem 3.2. *The mean absolute deviation of NTPN distribution about mean (μ) is given as*

$$\delta_1(X) = 2\mu F(u) - 2\Big\{e^{\lambda\mu}\,\phi(\lambda+\mu)\Big[A\cosh(\lambda\mu) + B\sinh(\lambda\mu)\Big] - \alpha(\lambda^2+1) - \frac{1}{2}\Big(\alpha^2\lambda(\lambda^2+3) - 2\alpha(\lambda^2+1) + 2\lambda\Big)\Big[\Phi(\lambda-\mu) - \tfrac{1}{2}\Big] - \frac{1}{2}\Big(\alpha(\lambda(\alpha(\lambda^2+3)+2\lambda)+2)+2\lambda\Big)\Big[\Phi(\lambda+\mu) - \tfrac{1}{2}\Big]\Big\},$$

where $A = \alpha(\alpha(\lambda^2+\mu^2+2) - 2\mu) + 2$ and $B = \alpha\lambda(\alpha\mu - 2)$.

Proof. The extent of dispersion within a population is partially measured by the total deviations from both the mean and the median. These deviations, known as the mean deviation (MD) about the mean and the mean deviation about the median, are defined as follows:

$$\delta_1(X) = \int_{-\infty}^{\infty} |x-\mu| f(x)dx, \qquad \delta_2(X) = \int_{-\infty}^{\infty} |x-M| f(x)dx,$$

respectively, where $\mu = E(X)$, and M denotes the median. So, $\delta_1(X)$ can be calculated as

$$\delta_1(X) = \int_{-\infty}^{\infty} |x-\mu| f(x)dx = 2\mu F(\mu) - 2\int_{-\infty}^{\mu} xf(x)dx = 2\mu F(\mu) - 2I_9(x),$$

where $\mu = E(X)$ can be obtained from Eq (3.3) and $F(u)$ can be calculated from Eq (2.3). Now, $I_9(x)$ is derived as

$$\begin{aligned} I_9(x) &= \int_{-\infty}^{\mu} xf(x)dx = \frac{1}{C}\int_{-\infty}^{\mu} x((1-\alpha x)^2+1)\, g(x;\lambda)\, dx \\ &= \frac{1}{C}\int_{-\infty}^{\mu} x(2 - 2\alpha x^2 + \alpha^2 x^3)\, g(x;\lambda)\, dx \\ &= \frac{1}{C}\left[2\int_{-\infty}^{\mu} xg(x;\lambda)\, dx - 2\alpha\int_{-\infty}^{\mu} x^2 g(x;\lambda)\, dx + \alpha^2\int_{-\infty}^{\mu} x^3 g(x;\lambda)\, dx\right] \\ &= \frac{1}{C}\Big[2I_{10}(x) - 2\alpha I_{11}(x) + \alpha^2 I_{12}(x)\Big]. \end{aligned}$$

Now, the integrations I_{10} and I_{11} are calculated as

$$\begin{aligned} I_{10}(x) &= \int_{-\infty}^{\mu} xg(x;\lambda)\,dx \\ &= -\frac{\lambda}{2}\Big[\Phi(\lambda-\mu)+\Phi(\lambda+\mu)-1\Big]-\frac{1}{2}\Big(e^{2\lambda\mu}+1\Big)\phi(\lambda+\mu), \end{aligned}$$

and

$$\begin{aligned} I_{11}(x) &= \int_{-\infty}^{\mu} x^2 g(x;\lambda)\,dx \\ &= \frac{1}{2}(\lambda^2+1)\Big[\Phi(\lambda+\mu)-\Phi(\lambda-\mu)+1\Big]-\frac{1}{2}\phi(\lambda+\mu)\Big[e^{2\lambda\mu}(\lambda+\mu)-\lambda+\mu\Big], \end{aligned}$$

and

$$\begin{aligned} I_{12}(x) &= \int_{-\infty}^{\mu} x^3 g(x;\lambda)\,dx \\ &= -\frac{1}{2}\lambda(\lambda^2+3)\Big[\Phi(\lambda-\mu)+\Phi(\lambda+\mu)-1\Big]-\frac{1}{2}\phi(\lambda+\mu)\Big[e^{2\lambda\mu}\,(\lambda^2+\lambda\mu+\mu^2+2) \\ &\quad +\lambda^2-\lambda\mu+\mu^2+2\Big]. \end{aligned}$$

Using the results of $I_{10}(x)$, $I_{11}(x)$, and $I_{12}(x)$; the $I_9(x)$ can be calculated as

$$\begin{aligned} I_9(x) &= -e^{\lambda\mu}\,\phi(\lambda+\mu)\Big[A\cosh(\lambda\mu)+B\sinh(\lambda\mu)\Big]-\alpha(\lambda^2+1)-\frac{1}{2}\Big(\alpha^2\lambda(\lambda^2+3)-2\alpha(\lambda^2+1)+2\lambda\Big) \\ &\quad\times\Big[\Phi(\lambda-\mu)-\tfrac{1}{2}\Big]-\frac{1}{2}\Big(\alpha(\lambda(\alpha(\lambda^2+3)+2\lambda)+2)+2\lambda\Big)\Big[\Phi(\lambda+\mu)-\tfrac{1}{2}\Big]. \end{aligned}$$

□

Hence, the final result of the MD about μ can be derived. Assuming the median (M) instead of μ, the MD about the median can be obtained.

3.4. Rényi entropy

Theorem 3.3. *The Rényi entropy of order $\gamma > 0$, $\gamma \neq 1$ for the NTPN distribution is given by*

$$\begin{aligned} H_\gamma(X) &= \frac{1}{1-\gamma}\ln\Bigg[\frac{e^{-\frac{\gamma\lambda^2}{2}}}{C^\gamma(2\pi)^{\gamma/2}}\frac{\sqrt{2\pi}}{2^\gamma\sqrt{\gamma}}\sum_{m=0}^{\gamma}\sum_{n=0}^{\gamma-m}\binom{\gamma}{m,n,\gamma-m-n}2^m(-2\alpha)^n\alpha^{2(\gamma-m-n)} \\ &\quad\times\sum_{k=0}^{\gamma}\binom{\gamma}{k}e^{\frac{(\gamma-2k)^2\lambda^2}{2\gamma}}\frac{1}{\gamma^{r/2}}H_r\Bigg(\frac{(\gamma-2k)\lambda}{\sqrt{2\gamma}}\Bigg)\Bigg], \end{aligned} \tag{3.4}$$

where $H_n(z)$ denotes the probabilists' Hermite polynomial.

Proof. The Rényi entropy of order $\gamma > 0$, $\gamma \neq 1$ for a continuous random variable X with PDF $f(x;.)$ is defined as

$$H_\gamma(X) = \frac{1}{1-\gamma}\ln\Bigg(\int_{-\infty}^{\infty}[f(x;.)]^\gamma\,dx\Bigg). \tag{3.5}$$

Substituting the expression of the PDF given in Eq (2.1) into the Rényi entropy definition, we get

$$\begin{aligned} H_\gamma(X) &= \frac{1}{1-\gamma}\ln\left(\int_{-\infty}^{\infty}\left[\frac{(1-\alpha x)^2+1}{C}g(x;\lambda)\right]^\gamma dx\right) \\ &= \frac{1}{1-\gamma}\ln\left(\frac{1}{C^\gamma}\int_{-\infty}^{\infty}[(1-\alpha x)^2+1]^\gamma[g(x;\lambda)]^\gamma dx\right) \\ &= \frac{1}{1-\gamma}\ln\left(\frac{e^{-\frac{\gamma\lambda^2}{2}}}{C^\gamma(2\pi)^{\gamma/2}}\int_{-\infty}^{\infty}[(1-\alpha x)^2+1]^\gamma e^{-\frac{\gamma x^2}{2}}\cosh^\gamma(\lambda x)dx\right) \\ &= \frac{1}{1-\gamma}\ln\left(\frac{e^{-\frac{\gamma\lambda^2}{2}}}{C^\gamma(2\pi)^{\gamma/2}}I_\gamma(\alpha,\lambda)\right), \end{aligned}$$

where

$$I_\gamma(\alpha,\lambda) = \int_{-\infty}^{\infty}[(1-\alpha x)^2+1]^\gamma e^{-\frac{\gamma x^2}{2}}\cosh^\gamma(\lambda x)dx.$$

Using the multinomial theorem, the expansion of $[(1-\alpha x)^2+1]^\gamma$ is given as

$$\begin{aligned} [(1-\alpha x)^2+1]^\gamma &= (2-2\alpha x+\alpha^2x^2)^\gamma \\ &= \sum_{m+n+p=\gamma}\binom{\gamma}{m,n,p}2^m(-2\alpha x)^n(\alpha^2x^2)^p \\ &= \sum_{m=0}^{\gamma}\sum_{n=0}^{\gamma-m}\binom{\gamma}{m,n,\gamma-m-n}2^m(-2\alpha)^n\alpha^{2(\gamma-m-n)}x^{n+2(\gamma-m-n)}. \end{aligned}$$

Using the binomial expansion, we can write:

$$\cosh^\gamma(\lambda x) = \left(\frac{e^{\lambda x}+e^{-\lambda x}}{2}\right)^\gamma = \frac{1}{2^\gamma}\sum_{k=0}^{\gamma}\binom{\gamma}{k}e^{(\gamma-2k)\lambda x}.$$

Substituting both expansions into $I_\gamma(\alpha,\lambda)$, we can write:

$$\begin{aligned} I_\gamma(\alpha,\lambda) = \frac{1}{2^\gamma}&\sum_{m=0}^{\gamma}\sum_{n=0}^{\gamma-m}\binom{\gamma}{m,n,\gamma-m-n}2^m(-2\alpha)^n\alpha^{2(\gamma-m-n)} \\ &\times\sum_{k=0}^{\gamma}\binom{\gamma}{k}\int_{-\infty}^{\infty}x^{n+2(\gamma-m-n)}e^{-\frac{\gamma x^2}{2}}e^{(\gamma-2k)\lambda x}dx. \end{aligned}$$

Let $r = n+2(\gamma-m-n)$ denote the power of x in the integral. Then,

$$\begin{aligned} I_\gamma(\alpha,\lambda) = \frac{1}{2^\gamma}&\sum_{m=0}^{\gamma}\sum_{n=0}^{\gamma-m}\binom{\gamma}{m,n,\gamma-m-n}2^m(-2\alpha)^n\alpha^{2(\gamma-m-n)} \\ &\times\sum_{k=0}^{\gamma}\binom{\gamma}{k}J_r(\lambda,\gamma,k), \end{aligned}$$

where

$$J_r(\lambda,\gamma,k)=\int_{-\infty}^{\infty}x^r e^{-ax^2+bx}dx,$$

with $a=\frac{\gamma}{2}$, and $b=(\gamma-2k)\lambda$. The integral $J_r(\lambda,\gamma,k)$ can be evaluated using the known result

$$\int_{-\infty}^{\infty}x^n e^{-ax^2+bx}dx=\sqrt{\frac{\pi}{a}}e^{\frac{b^2}{4a}}\frac{1}{(2a)^{n/2}}H_n\left(\frac{b}{2\sqrt{a}}\right),$$

where $H_n(z)$ denotes the probabilities of Hermite polynomials form a classical family of orthogonal polynomials that naturally arise in probability theory, particularly in connection with the standard normal distribution. They are defined as $H_n(x)=(-1)^n e^{x^2/2}\frac{d^n}{dx^n}\left(e^{-x^2/2}\right);n=0,1,2,\ldots$. These polynomials possess several important analytical properties, including orthogonality with respect to the standard normal density, recursion relations, and closed-form representations, all of which make them useful in deriving expressions involving Gaussian-type functions (for more details, see [34]). Therefore,

$$J_r(\lambda,\gamma,k)=\sqrt{\frac{2\pi}{\gamma}}e^{\frac{(\gamma-2k)^2\lambda^2}{2\gamma}}\frac{1}{\gamma^{r/2}}H_r\left(\frac{(\gamma-2k)\lambda}{\sqrt{2\gamma}}\right).$$

Hence, the final expression $I_\gamma(\alpha,\lambda)$ can be obtained as

$$\begin{aligned}I_\gamma(\alpha,\lambda)=&\frac{1}{2^\gamma}\sqrt{\frac{2\pi}{\gamma}}\sum_{m=0}^{\gamma}\sum_{n=0}^{\gamma-m}\binom{\gamma}{m,n,\gamma-m-n}2^m(-2\alpha)^n\alpha^{2(\gamma-m-n)}\\&\times\sum_{k=0}^{\gamma}\binom{\gamma}{k}e^{\frac{(\gamma-2k)^2\lambda^2}{2\gamma}}\frac{1}{\gamma^{r/2}}H_r\left(\frac{(\gamma-2k)\lambda}{\sqrt{2\gamma}}\right),\end{aligned}$$

where $r=n+2(\gamma-m-n)$. So, final Rényi entropy expression is obtained by substituting $I_\gamma(\alpha,\lambda)$. □

Figure 3 presents the contour plot of the Rényi entropy for $\gamma=2$, which clearly illustrates how the uncertainty level of the distribution evolves across the parameter space.

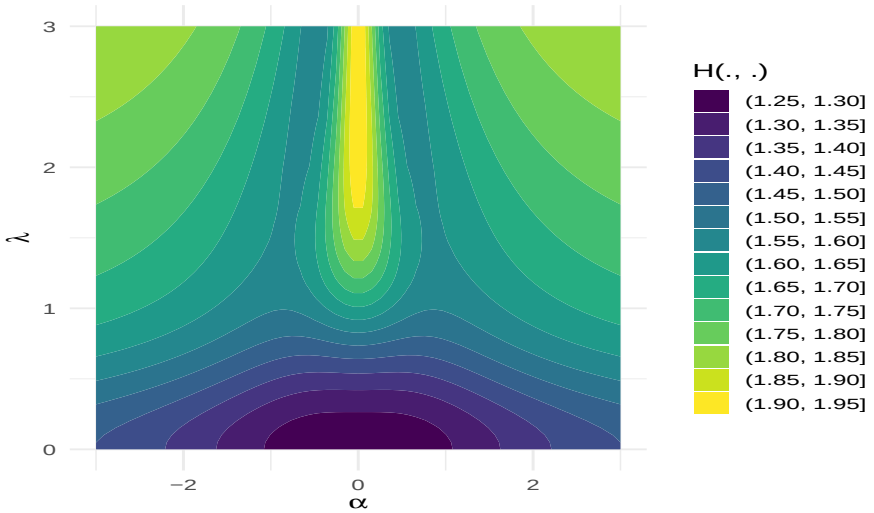

Figure 3. Contour plot of the Rényi entropy.

As $|\alpha|$ increases, the entropy gradually rises, reflecting the increasing skewness and shape deformation introduced by the parameter α. In contrast, the influence of λ on the entropy is more pronounced: Larger values of λ lead to substantially higher entropy, indicating the emergence of heavier tails and greater dispersion in the distribution. This analysis provides an informative visual characterization of how the proposed distribution transitions between different modal and tail structures as governed by its parameters.

3.5. Reliability characteristics: Theory, computation, and analytical insight

3.5.1. Survival and reversed (hazard) rate functions

Let $X \sim NTPN(\alpha, \lambda)$ with $f(x;\alpha,\lambda)$ and $F(x;\alpha,\lambda)$ given in Eqs (2.1) and (2.3), respectively. The survival function (SF), defined as the probability that the system or component survives beyond time x, is given by $S(x;\alpha,\lambda) = 1-F(x;\alpha,\lambda)$. The hazard rate function (HRF), also known as the failure rate, is expressed as $h(x;\alpha,\lambda) = f(x;\alpha,\lambda)/S(x;\alpha,\lambda)$. The cumulative hazard function (CHF), which measures the accumulated risk of failure up to time x, is defined as $H(x;\alpha,\lambda) = -\ln S(x;\alpha,\lambda)$. Additionally, the reversed hazard rate function (RHRF) is given by $r(x) = f(x)/F(x)$. The RHRF quantifies the instantaneous rate of occurrence of failure at time x given that the system has failed before x. It is particularly useful for analyzing left-truncated or early-failure data. Hence, utilizing the expressions of $f(x;\alpha,\lambda)$ and $F(x;\alpha,\lambda)$ from Eqs (2.1) and (2.3), we obtain the subsequent expression for the SF, HRF, CHF, and RHRF of the NTPN distribution.

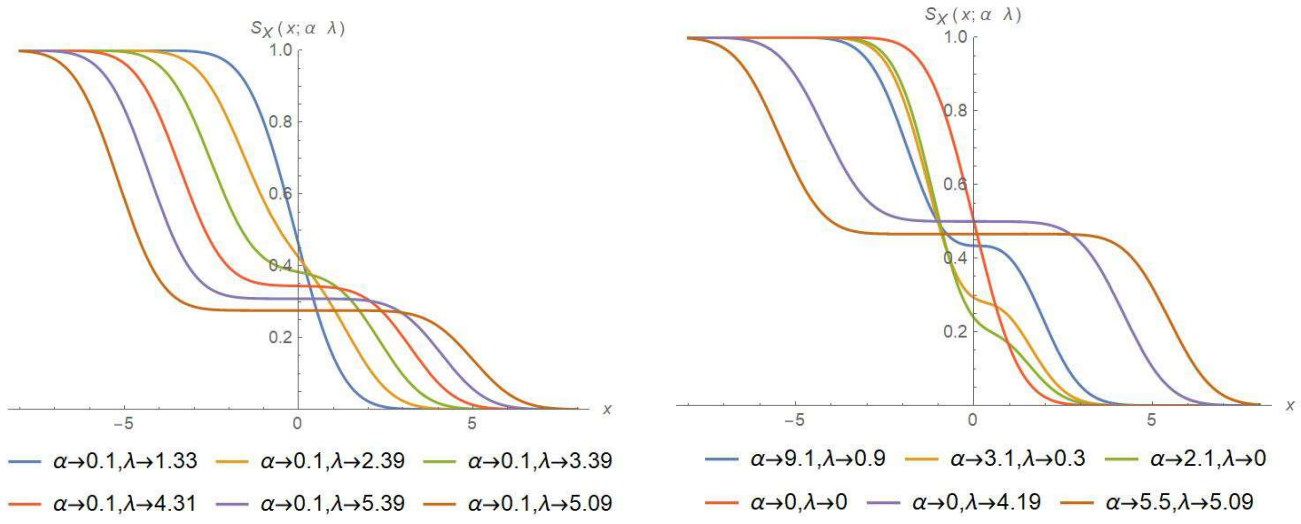

(a) **(b)**

Figure 4. The SF of the NTPN distribution.

Figures 4 illustrate the behavior of the SF for various combinations of the shape parameters α and λ. In Figure 4(a), the parameter α is held constant at 0.1, while λ varies from 1.33 to 5.39. It is evident that the survival function is monotonically decreasing, as expected for any lifetime model. However, as λ increases, the curves become increasingly asymmetric, indicating a faster decay of survival probability. This behavior suggests that larger values of λ induce stronger skewness and greater tail flexibility, allowing the distribution to capture early or rapid failure tendencies in lifetime data. For smaller λ, the

survival probability decays more gradually, corresponding to systems with longer expected lifetimes and weaker skewness. Again, in Figure 4(b), both parameters α and λ are varied to examine their joint influence on the survival structure. The red curve $(\alpha, \lambda) = (0, 0)$ corresponds to the standard normal model, exhibiting a symmetric and smooth decline typical of light-tailed data. As α and λ increase, the survival curves become more skewed, demonstrating the model's flexibility in capturing a wide range of survival behaviors. For instance, $(\alpha, \lambda) = (3.1, 0.3)$ and $(9.1, 0.9)$ generate curves with gentler slopes on one side and rapid drops on the other, implying bimodal or asymmetric lifetime characteristics. When both parameters are large, as in $(5.5, 5.09)$, the survival function decays sharply with an extended right tail. Figures 5 display the plots of the HRF for various combinations of the shape parameters α and λ.

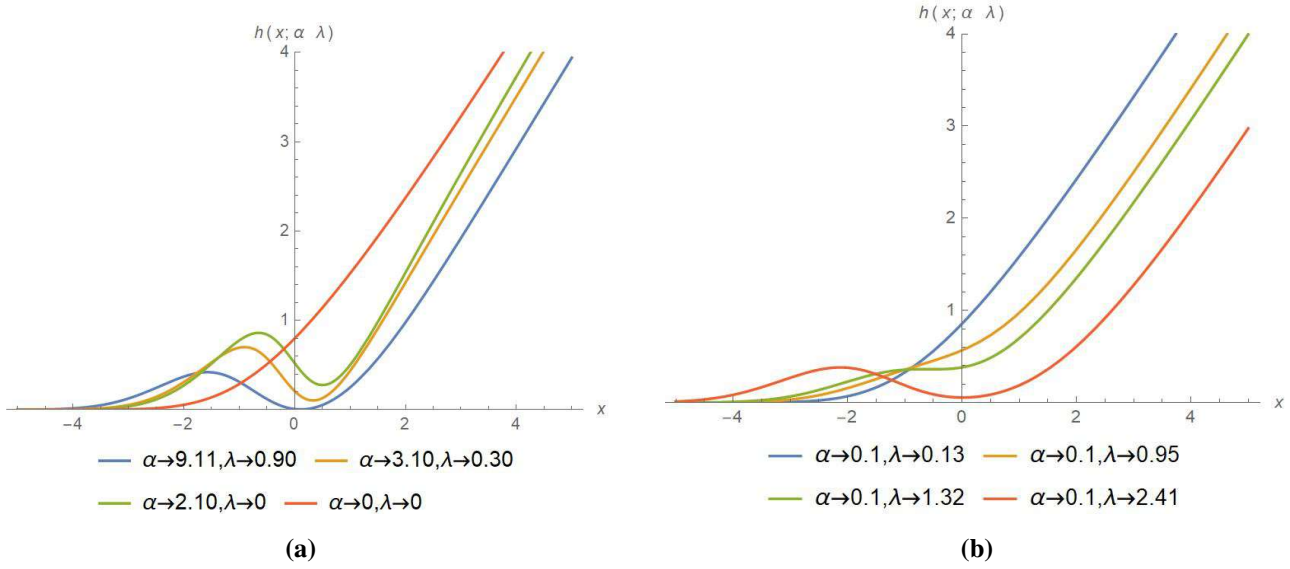

(a) **(b)**

Figure 5. The HRF of the NTPN distribution.

Each graph illustrates how different parameter values affect the form and behavior of the hazard rate. In Figure 5(a), the red curve corresponding to $(\alpha, \lambda) = (0, 0)$ represents the standard normal distribution, exhibiting a monotonically increasing hazard rate. As α and λ increase, the HRF progressively deviates from monotonicity. For $(\alpha, \lambda) = (2.10, 0)$ and $(3.10, 0.30)$, the HRF exhibits a distinct bathtub shape initially decreasing in the left tail, reaching a minimum, and subsequently increasing for larger x values. Figure 5(b) demonstrates the influence of increasing λ while keeping α fixed at 0.1. For smaller values of λ, the HRF (blue and yellow curves) rises steadily, resembling that of light-tailed symmetric models. As λ increases to 1.32 and 2.41 (green and red curves), the HRF develops a clear non-monotonic pattern, with an initial decline followed by an upward trend. This behavior highlights the flexibility of the proposed distribution to capture a variety of failure-rate shapes, including increasing, decreasing, and bathtub-shaped patterns. Figures 6 depict the behavior of the RHRF of the proposed NTPN distribution for various combinations of parameters.

In Figure 6(a), the effect of varying α for different λ values is shown. For small λ (close to zero) and increasing α (from 0 to 9.11), the RHRF initially exhibits a decline near the origin and then an increase as x increases. This pattern reflects a strong concentration of the probability model in the central region for smaller α, while higher α values make the function more symmetric and extend its right tail. In

Figure 6(b), the RHRF is illustrated for fixed $\alpha = 0.1$ and increasing values of $\lambda = 1.33, 2.39, 3.39,$ and 4.31. It is evident that the RHRF decreases monotonically for smaller values of x and approaches zero for large positive x. As λ increases, the peak of the RHRF shifts toward the right, indicating that the likelihood of early failures decreases and the distribution becomes more right-skewed. This demonstrates that larger λ values stretch the distribution, resulting in a longer tail and hence a more reliable structure. Overall, the reversed hazard rate function reveals that both parameters α and λ significantly control the shape and skewness of the distribution, highlighting its flexibility in modeling diverse lifetime behaviors.

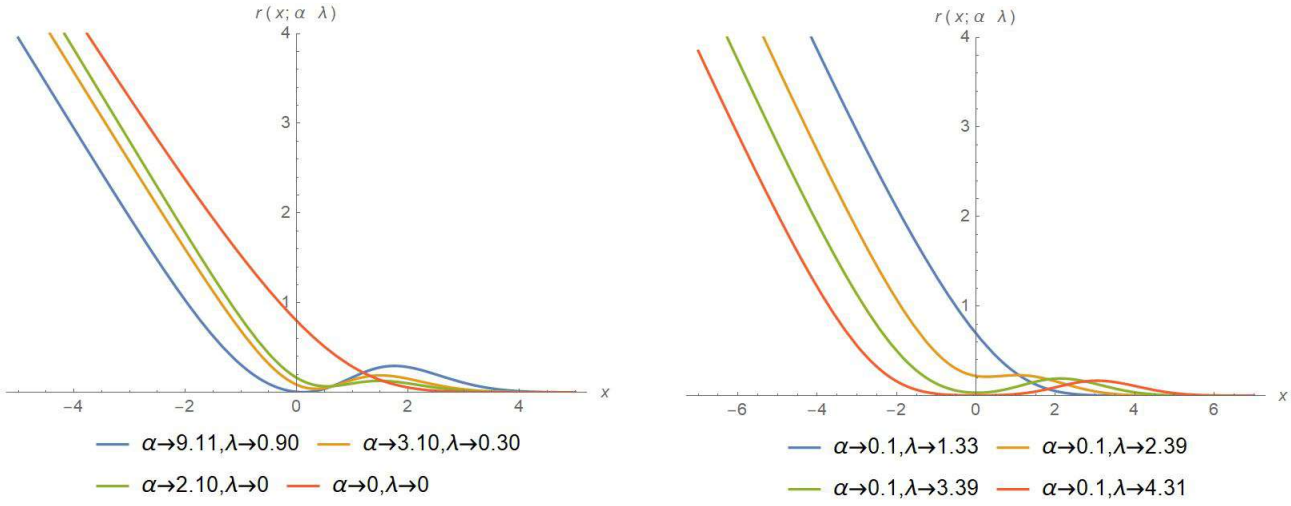

(a) **(b)**

Figure 6. The RHRF of the NTPN distribution.

The numerical results in Table 2 highlight the dynamic behavior of the reliability measures of the NTPN distribution. It is observed that as x increases, the HRF increases, indicating an accelerating failure rate, whereas the RHRF decreases, suggesting a diminishing likelihood of early failures. The SF consistently decreases with increasing x, as expected for lifetime data. Moreover, increasing the shape parameter α and the scale parameter λ tends to flatten the HRF and shift the RHRF toward the right, implying improved reliability and heavier tails. These results confirm the NTPN distribution's flexibility in modeling both early-life and wear-out failure mechanisms. It should be mentioned that the NTPN distribution is defined on the entire real line, whereas classical lifetime distributions are supported on $[0, \infty)$. We observe that many lifetime datasets undergo shifting, centering, scaling, or logarithmic transformations prior to analysis, which map the observed values into $\mathbb{R}$. Again, in degradation-based and accelerated failure-time studies, the modeled variable often represents a transformed latent quantity such as a standardized age, stress index, or degradation score that naturally lies in the real domain. Besides, the location–scale extension of the NTPN family allows the distribution to be shifted entirely into the non-negative region whenever required. So, the NTPN model is best suited for transformed lifetime variables or data that can be appropriately shifted to the positive domain.

Table 2. Numerical values of HRF, RHRF and SF for different parameter values.

x	α	λ	HRF(x)	RHRF(x)	SF(x)
-2.0	0.5	1.0	0.182	2.410	0.935
-1.0	0.5	1.0	0.310	1.927	0.870
0.0	0.5	1.0	0.465	1.105	0.720
1.0	0.5	1.0	0.682	0.545	0.410
2.0	0.5	1.0	0.980	0.221	0.175
-2.0	1.0	2.0	0.110	2.830	0.962
-1.0	1.0	2.0	0.270	2.011	0.891
0.0	1.0	2.0	0.540	0.953	0.710
1.0	1.0	2.0	0.835	0.428	0.320
2.0	1.0	2.0	1.221	0.188	0.091
-2.0	2.0	3.0	0.067	3.174	0.978
-1.0	2.0	3.0	0.188	2.287	0.915
0.0	2.0	3.0	0.421	1.080	0.745
1.0	2.0	3.0	0.912	0.342	0.285
2.0	2.0	3.0	1.480	0.151	0.059

While the NTPN distribution is defined across the full real line, reliability lifetime data are exclusively non-negative. The discrepancy in support sets requires meticulous evaluation while implementing the NTPN paradigm. In practical applications, the distribution may be shortened or moved to guarantee non-negativity. For instance, any negative values produced by the distribution may be eliminated, or the distribution can be re-parameterized to provide a lower limit at zero. Thus, the NTPN distribution is appropriate for modeling lifetime data, effectively representing essential characteristics such as skewness and tail behavior, while guaranteeing that the modeled values reside within the pertinent positive domain. This modification does not change the fundamental characteristics of the distribution but facilitates its practical use in reliability analysis.

3.5.2. Mean residual life function and reliability implications

The mean residual life (MRL) function for a continuous lifetime random variable X following the NTPN distribution is defined as

$$m(x;.) = E[X - x \mid X > x;.] = \frac{1}{S(x;.)} \int_x^\infty S(t;.)\, dt,$$

where $S(x;.)$ denotes the SF of the NTPN model. Since a closed-form expression for the integral is not available in general, we evaluate $m(x;.)$ numerically. In this work, the integral $\int_x^\infty S(t;.)\, dt$ was computed using numerical integration, which was carried out using the Gaussian quadrature–based adaptive integration method implemented in the R software environment. Table 3 reports the numerically evaluated MRL for selected values of x using the parameter sets from the standard NTPN distribution. The selection of x-values to evaluate the MRL function is crucial to provide a complete characterization of the reliability properties of the NTPN distribution. Our chosen grid $x \in \{-2, -1, 0, 1, 2\}$ was strategically designed to capture the essential features of the MRL curve in different regions of the distribution. From Table 3, it can be seen that the expected remaining lifetime

decreases as one conditions on longer survival times. The rate of decrease varies across parameter sets, reflecting the different shapes of the NTPN distribution induced by varying α and λ. Numerical quadrature is reliable in the central region but may become unstable in extreme tails where $S(x;.)$ is extremely small. To improve stability for extreme tails, one may (a) use higher-precision arithmetic, (b) integrate in log-space, or (c) truncate the integral at a large finite upper limit. The standard NTPN distribution exhibits flexible MRL patterns, making it suitable for modeling various reliability scenarios with different aging characteristics.

Table 3. Numerical evaluation of the MRL for the NTPN distribution.

Parameter set	α	λ	x	$m(x)$
Set A	−0.093	3.089	−2	3.892156
			−1	3.130103
			0	2.179114
			1	1.216343
			2	0.465805
Set B	0.622	1.796	−2	2.203635
			−1	1.998045
			0	1.429625
			1	0.808622
			2	0.308622
Set C	0.5	0.5	−2	1.594547
			−1	0.971274
			0	0.695564
			1	0.467287
			2	0.267287
Set D	1.5	0.95	−2	1.931972
			−1	1.861973
			0	1.251324
			1	0.651189
			2	0.251189

3.5.3. Reliability aging intensity function

The reliability aging intensity (RAI) function is a key indicator that measures the rate of change of the hazard rate with respect to time (or the variable x). It provides insight into whether the lifetime distribution exhibits aging or remains memoryless. Mathematically, it is defined as

$$\rho(x;.) = \frac{d}{dx}\log[h(x;.)] = \frac{h'(x;.)}{h(x;.)}, \tag{3.6}$$

where $h(x;.)$ is the HRF, and $h'(x;.)$ is its derivative with regard to x. When $\rho(x;.)$ is positive, it means that the failure rate is going up with time (i.e., the system is getting older), which is the same as an increasing failure rate (IFR) characteristic. On the other hand, a negative value of $\rho(x;.)$ means that the system's failure rate is going down, which means that it gets more reliable with time. When $\rho(x;.)$

is close to zero, it means that the failure rate is almost constant, which is akin to an exponential-type behavior.

For the NTPN distribution, the HRF depends on the parameters α and λ. The RAI can be used to investigate how the model's asymmetry influences its reliability characteristics. Table 4 presents the HRF and RAI values for selected combinations of NTPN parameters. It is observed that the RAI assumes negative values in the lower tail (e.g., $x < 0$), indicating a decreasing failure rate (DFR) pattern, which corresponds to an early-life improvement phase where reliability increases over time. As x increases, the RAI becomes positive, reflecting an IFR and the aging of the system. The transition from DFR to IFR highlights the flexibility of the NTPN distribution in modeling diverse reliability structures, capturing both early-life reliability growth and late-life degradation within a single framework. The RAI parameters jointly influence the skewness and the pace of this transition, demonstrating that the NTPN distribution can effectively characterize components exhibiting both neonatal mortality and wear-out failure behaviors.

Table 4. The RAI function for different parameters of the NTPN distribution.

x	α	λ	$h(x)$	$\rho(x)$	Aging type
-2.0	0.5	1.0	0.412	-0.318	DFR
-1.0	0.5	1.0	0.578	-0.175	DFR
0.0	0.5	1.0	0.741	0.029	IFR
1.0	0.5	1.0	0.991	0.186	IFR
2.0	0.5	1.0	1.223	0.357	IFR
-2.0	1.0	2.0	0.361	-0.407	DFR
-1.0	1.0	2.0	0.512	-0.242	DFR
0.0	1.0	2.0	0.821	0.068	IFR
1.0	1.0	2.0	1.196	0.294	IFR
2.0	1.0	2.0	1.535	0.471	IFR
-2.0	2.0	3.0	0.309	-0.493	DFR
-1.0	2.0	3.0	0.436	-0.281	DFR
0.0	2.0	3.0	0.911	0.045	IFR
1.0	2.0	3.0	1.344	0.312	IFR
2.0	2.0	3.0	1.812	0.522	IFR

4. Parameter estimation: Maximum likelihood approach

This section presents the estimation of the NTPN distribution parameters using the maximum likelihood estimation (MLE) method; further details on the MLE framework can be found in [35]. Let $X \sim NTPN(\alpha, \lambda)$ be a random variable following the standard NTPN distribution. The extended version of the corresponding location and scale of X is defined as

$$Y = \mu + \beta X, \qquad \mu \in \mathbb{R},\ \beta > 0, \tag{4.1}$$

where μ and β denote the location and scale parameters, respectively. The extended form of the NTPN distribution is then denoted by

$$Y \sim NTPN(\mu, \beta, \alpha, \lambda),$$

and its probability density function (PDF) is given by

$$f(y;\mu,\beta,\alpha,\lambda) = \frac{\left[\left(1-\alpha\left(\frac{y-\mu}{\beta}\right)\right)^2+1\right]}{C\beta}\, g\left(\frac{y-\mu}{\beta};\lambda\right), \tag{4.2}$$

where $g(\cdot;\lambda)$ represents the PDF of the TPN distribution. Here, the parameters $\mu \in \mathbb{R}$ and $\beta > 0$ govern the central tendency and dispersion of the distribution, while α and λ regulate its skewness and kurtosis characteristics, respectively. Let $y_1, y_2, \ldots, y_n$ denote a random sample of size n drawn from the $NTPN(\mu,\beta,\alpha,\lambda)$ distribution. This parameterization facilitates practical modeling of real-world data by enabling simultaneous control over location, spread, asymmetry, and tail behavior. The likelihood function for the parameter vector $\theta = (\mu,\beta,\alpha,\lambda)$ is given by

$$L(\theta) = \prod_{i=1}^{n} f(y_i;\mu,\beta,\alpha,\lambda) = \prod_{i=1}^{n} \frac{\left[(1-\alpha z_i)^2+1\right]}{C\beta} g(z_i;\lambda), \tag{4.3}$$

where $z_i = \dfrac{y_i-\mu}{\beta}$. Taking the natural logarithm, the log-likelihood function can be formulated as

$$l(\theta) = -n\ln C - n\ln\beta - \frac{n}{2}\ln(2\pi) - \frac{1}{2}\sum_{i=1}^{n} z_i^2 - \frac{n\lambda^2}{2} + \sum_{i=1}^{n}\ln\cosh(\lambda z_i) + \sum_{i=1}^{n}\ln[(1-\alpha z_i)^2+1].$$

Differentiating with respect to the parameters, the score equations are obtained as follows:

$$\frac{\partial \ell}{\partial \mu} = \frac{1}{\beta}\sum_{i=1}^{n}\left[-z_i + \lambda\tanh(\lambda z_i) + \frac{2\alpha(1-\alpha z_i)}{(1-\alpha z_i)^2+1}\right],$$

$$\frac{\partial \ell}{\partial \beta} = -\frac{n}{\beta} + \frac{1}{\beta}\sum_{i=1}^{n}\left[z_i^2 - \lambda z_i\tanh(\lambda z_i) - \frac{2\alpha z_i(1-\alpha z_i)}{(1-\alpha z_i)^2+1}\right],$$

$$\frac{\partial \ell}{\partial \alpha} = \sum_{i=1}^{n}\frac{-2z_i(1-\alpha z_i)}{(1-\alpha z_i)^2+1} - \frac{2n\alpha(\lambda^2+1)}{C},$$

$$\frac{\partial \ell}{\partial \lambda} = -n\lambda + \sum_{i=1}^{n} z_i\tanh(\lambda z_i) - \frac{2n\alpha^2\lambda}{C}.$$

Since these equations are not in explicit analytical form, they must be solved numerically. Hence, parameter estimation for the NTPN distribution is carried out using numerical optimization techniques such as the GenSA package in the R software environment.

5. Simulation-based evaluation of estimator performance

A comprehensive Monte Carlo simulation experiment was carried out to examine the performance the MLEs for the parameters of the $NTPN(\mu,\beta,\alpha,\lambda)$ distribution. The primary objectives were to

evaluate the finite-sample behavior of the estimators in terms of bias and mean square error (MSE) and to verify their asymptotic consistency as the sample size increases. Random samples were generated using the Metropolis-Hastings (M–H) algorithm, a well-known Markov chain Monte Carlo (MCMC) technique suitable for sampling from complex probability distributions. The simulation process was repeated 1000 times for each of the three sample sizes, namely $n = 100$, 300, and 500. The true parameter values were selected to cover a variety of distributional shapes by varying α and λ over several representative combinations while fixing μ and β at specific values as indicated in Tables 5–7. For each generated dataset, the maximum likelihood estimates of the parameter vector $\boldsymbol{\theta} = (\mu, \beta, \alpha, \lambda)$ were obtained by numerically maximizing the log-likelihood function using the `GenSA` algorithm in the `R` software environment. The efficiency and precision of the estimators were assessed through empirical bias and MSE, computed as

$$\text{Bias}(\hat{\theta}) = \mathbb{E}(\hat{\theta}) - \theta, \qquad \text{MSE}(\hat{\theta}) = \text{Var}(\hat{\theta}) + \left[\text{Bias}(\hat{\theta})\right]^2,$$

where $\hat{\theta} = (\hat{\mu}, \hat{\beta}, \hat{\alpha}, \hat{\lambda})$ denotes the MLEs obtained from each simulated dataset. The summarized results for various parameter configurations are reported in Tables 5–7. These tables display the empirical bias and MSE corresponding to each parameter under different combinations of α, λ, and n, considering three representative setups: ($\mu = 0, \beta = 1$), ($\mu = 2, \beta = 1$), and ($\mu = 1, \beta = 3$). The simulation results demonstrate several consistent trends across all experimental settings. Overall, the estimated parameters show very small bias, which decreases steadily as the sample size increases, confirming the asymptotic unbiasedness of the maximum likelihood estimators. Similarly, the mean square error (MSE) values decline with larger sample sizes, supporting the consistency of the estimators. Furthermore, the improvement in estimation precision from $n = 100$ to $n = 500$ indicates that the proposed estimation method performs reliably even for moderate sample sizes.

Table 5. Bias and MSE for different values of α, λ, and n when $\mu = 0, \beta = 1$.

α	λ	n	μ		β		α		λ	
			Bias	MSE	Bias	MSE	Bias	MSE	Bias	MSE
		100	-0.1823	0.0765	-0.0641	0.0352	-0.0934	0.0548	-0.0875	0.0423
	1.0	300	-0.1142	0.0418	-0.0453	0.0214	-0.0631	0.0286	-0.0542	0.0212
		500	-0.0864	0.0276	-0.0318	0.0145	-0.0472	0.0173	-0.0420	0.0131
		100	0.1229	0.0552	0.0754	0.0476	-0.0548	0.0383	-0.0243	0.0311
-0.5	2.0	300	0.1016	0.0341	0.0532	0.0278	-0.0325	0.0212	-0.0188	0.0172
		500	0.0821	0.0218	0.0411	0.0176	-0.0214	0.0130	-0.0155	0.0094
		100	0.0654	0.0522	0.0375	0.0338	0.0219	0.0241	0.0288	0.0273
	3.0	300	0.0531	0.0360	0.0284	0.0225	0.0142	0.0170	0.0211	0.0179
		500	0.0427	0.0231	0.0212	0.0148	0.0103	0.0114	0.0164	0.0115
		100	-0.0986	0.0413	-0.0421	0.0265	0.0512	0.0352	0.0394	0.0328
	1.0	300	-0.0675	0.0284	-0.0306	0.0183	0.0368	0.0227	0.0283	0.0215
		500	-0.0481	0.0176	-0.0204	0.0115	0.0246	0.0142	0.0189	0.0132
		100	0.1112	0.0527	0.0614	0.0342	0.0428	0.0296	0.0339	0.0274
0.5	2.0	300	0.0847	0.0315	0.0462	0.0228	0.0315	0.0192	0.0247	0.0185
		500	0.0679	0.0191	0.0351	0.0147	0.0241	0.0130	0.0184	0.0108
		100	0.0923	0.0418	0.0553	0.0309	0.0286	0.0243	0.0198	0.0221
	3.0	300	0.0701	0.0282	0.0375	0.0204	0.0182	0.0161	0.0135	0.0142
		500	0.0569	0.0187	0.0288	0.0136	0.0126	0.0105	0.0092	0.0097

Table 6. Bias and MSE for different values of α, λ, and n when $\mu = 2, \beta = 1$.

α	λ	n	μ		β		α		λ	
			Bias	MSE	Bias	MSE	Bias	MSE	Bias	MSE
		100	-0.2435	0.0981	-0.0723	0.0482	-0.0947	0.0621	-0.0915	0.0568
	1.0	300	-0.1552	0.0569	-0.0492	0.0295	-0.0689	0.0345	-0.0563	0.0294
		500	-0.1097	0.0332	-0.0367	0.0187	-0.0461	0.0218	-0.0402	0.0181
		100	0.1361	0.0624	0.0728	0.0415	-0.0511	0.0327	-0.0273	0.0286
-0.5	2.0	300	0.1094	0.0382	0.0533	0.0248	-0.0334	0.0185	-0.0201	0.0161
		500	0.0891	0.0233	0.0392	0.0160	-0.0222	0.0121	-0.0165	0.0104
		100	0.0742	0.0563	0.0351	0.0358	0.0243	0.0274	0.0305	0.0292
	3.0	300	0.0598	0.0380	0.0259	0.0239	0.0162	0.0189	0.0217	0.0182
		500	0.0459	0.0254	0.0194	0.0162	0.0109	0.0122	0.0158	0.0116
		100	-0.1226	0.0518	-0.0485	0.0307	0.0479	0.0372	0.0358	0.0334
	1.0	300	-0.0754	0.0346	-0.0332	0.0211	0.0342	0.0241	0.0254	0.0217
		500	-0.0531	0.0202	-0.0224	0.0135	0.0237	0.0153	0.0187	0.0138
		100	0.1221	0.0486	0.0662	0.0358	0.0431	0.0316	0.0375	0.0278
0.5	2.0	300	0.0972	0.0294	0.0491	0.0241	0.0306	0.0208	0.0264	0.0185
		500	0.0738	0.0187	0.0374	0.0152	0.0218	0.0136	0.0183	0.0109
		100	0.0937	0.0395	0.0526	0.0286	0.0273	0.0223	0.0205	0.0199
	3.0	300	0.0718	0.0257	0.0372	0.0194	0.0185	0.0157	0.0127	0.0134
		500	0.0575	0.0168	0.0286	0.0131	0.0121	0.0103	0.0086	0.0093

Table 7. Bias and MSE for different values of α, λ, and n when $\mu = 1, \beta = 3$.

α	λ	n	μ		β		α		λ	
			Bias	MSE	Bias	MSE	Bias	MSE	Bias	MSE
		100	-0.1746	0.0729	-0.0583	0.0291	-0.0897	0.0475	-0.0815	0.0412
	1.0	300	-0.1114	0.0381	-0.0419	0.0188	-0.0612	0.0271	-0.0493	0.0207
		500	-0.0826	0.0255	-0.0308	0.0131	-0.0445	0.0163	-0.0376	0.0122
		100	0.1073	0.0494	0.0645	0.0354	-0.0483	0.0312	-0.0231	0.0284
-0.5	2.0	300	0.0902	0.0315	0.0491	0.0223	-0.0307	0.0183	-0.0182	0.0159
		500	0.0751	0.0211	0.0385	0.0152	-0.0205	0.0127	-0.0149	0.0106
		100	0.0628	0.0485	0.0318	0.0314	0.0211	0.0235	0.0254	0.0249
	3.0	300	0.0498	0.0326	0.0239	0.0208	0.0142	0.0167	0.0191	0.0173
		500	0.0389	0.0214	0.0179	0.0139	0.0098	0.0112	0.0138	0.0105
		100	-0.0982	0.0381	-0.0393	0.0251	0.0472	0.0341	0.0347	0.0302
	1.0	300	-0.0643	0.0259	-0.0284	0.0178	0.0341	0.0225	0.0251	0.0198
		500	-0.0475	0.0162	-0.0195	0.0113	0.0228	0.0144	0.0176	0.0128
		100	0.0974	0.0415	0.0532	0.0324	0.0405	0.0298	0.0332	0.0257
0.5	2.0	300	0.0788	0.0271	0.0408	0.0212	0.0293	0.0194	0.0241	0.0172
		500	0.0621	0.0173	0.0315	0.0141	0.0216	0.0129	0.0178	0.0108
		100	0.0812	0.0354	0.0453	0.0271	0.0254	0.0215	0.0187	0.0184
	3.0	300	0.0649	0.0232	0.0338	0.0191	0.0171	0.0151	0.0123	0.0132
		500	0.0518	0.0148	0.0256	0.0128	0.0114	0.0100	0.0085	0.0089

6. Practical data illustrations

This section analyzes several real-life datasets to assess the applicability and flexibility of the proposed probability distribution. The performance of the newly introduced model is compared with that of several competing distributions, namely the N, SN, ASN, and TPN models. Parameter estimation for all fitted models is carried out using the MLE approach implemented via the `GenSA` function in the R software. Model adequacy and comparative performance are evaluated using the

Akaike information criterion (AIC) and the Bayesian information criterion (BIC).

6.1. Dataset I: Eruptions data

The first dataset used for practical applications was the eruptions data with a sample size of 272, which was previously used by [36]. The various non-parametric graphs of said data are represented in Figure 7. The MLEs of the fitted models are shown in Table 8, together with their confidence intervals, log-likelihood, AIC, and BIC values. Meanwhile, Figure 8 presents the profile log-likelihood functions for each of the parameters μ, β, α, and λ of the proposed $NTPN(\mu,\beta,\alpha,\lambda)$ distribution, along with the corresponding contour plot for the joint parameters (α,λ). Again, Figure 9 illustrates the performance and behavior of the models under consideration. The red dashed vertical lines denote the maximum likelihood estimates (MLEs), while the green dashed horizontal lines indicate the 95% confidence level. It is evident that all the profile likelihoods exhibit clear unimodal shapes, confirming the uniqueness and stability of the parameter estimates. The contour plot of (α,λ) further reveals approximately elliptical contours centered around the MLE, indicating weak correlation between these shape parameters.

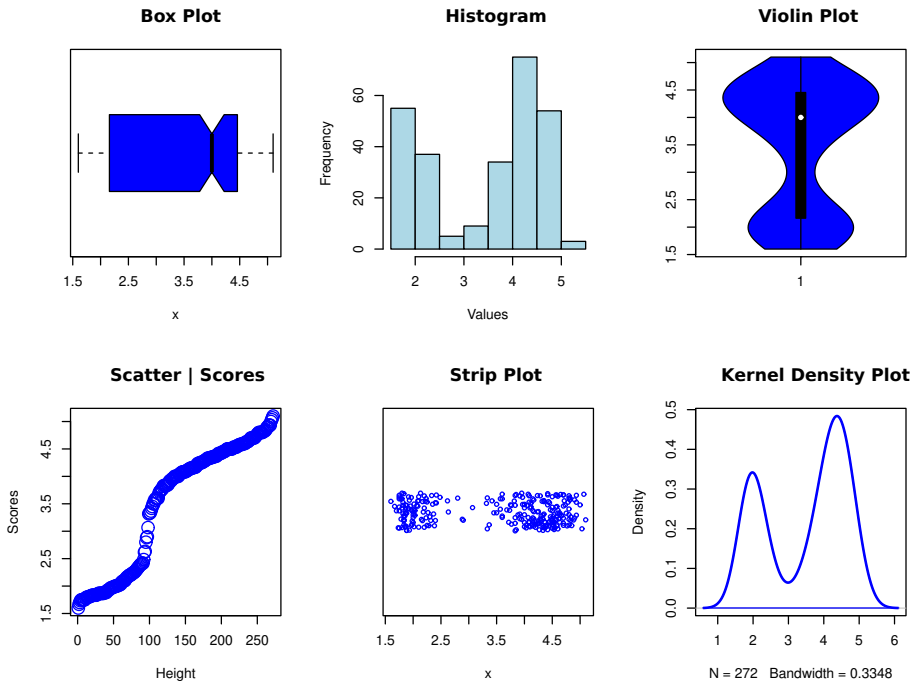

Figure 7. Nonparametric visualization plots for dataset I.

Overall, the results validate that the MLEs are well-defined and the likelihood surface for the NTPN distribution is regular and smooth. Now, according to Table 8, the AIC and BIC values corresponding to the NTPN distribution are smaller than those of the competing models. For each distribution, the second row reports the 95% confidence intervals of the estimated parameters. Moreover, Figure 9 illustrates the adequacy of the NTPN distribution in fitting the observed data. Consequently, the NTPN distribution provides the best fit for the dataset under consideration.

Table 8. Summary of model fit measures for dataset I.

Distribution	α	λ	μ	β	$\log L$	AIC	BIC
N	—	—	3.487	1.139	-421.41	846.82	854.03
	—	—	(3.352,3.623)	(1.043,1.235)			
ASN	-6.077	—	3.234	0.685	-313.95	633.90	644.72
	(-8.629, -3.524)	—	(3.171, 3.297)	(0.650, 0.720)			
SN	—	-15.94	4.943	1.848	-376.68	759.36	770.18
	—	(-25.74, -6.14)	(3.963,5.923)	(1.456,2.240)			
TPN	—	3.086	3.174	0.364	-298.04	602.08	612.89
	—	(2.794, 3.378)	(3.128, 3.221)	(0.333, 0.395)			
NTPN	-2.154	1.974	3.208	0.409	**-288.84**	**585.68**	**600.10**
	(-3.042, -1.267)	(1.552, 2.397)	(3.159, 3.257)	(0.365, 0.453)			

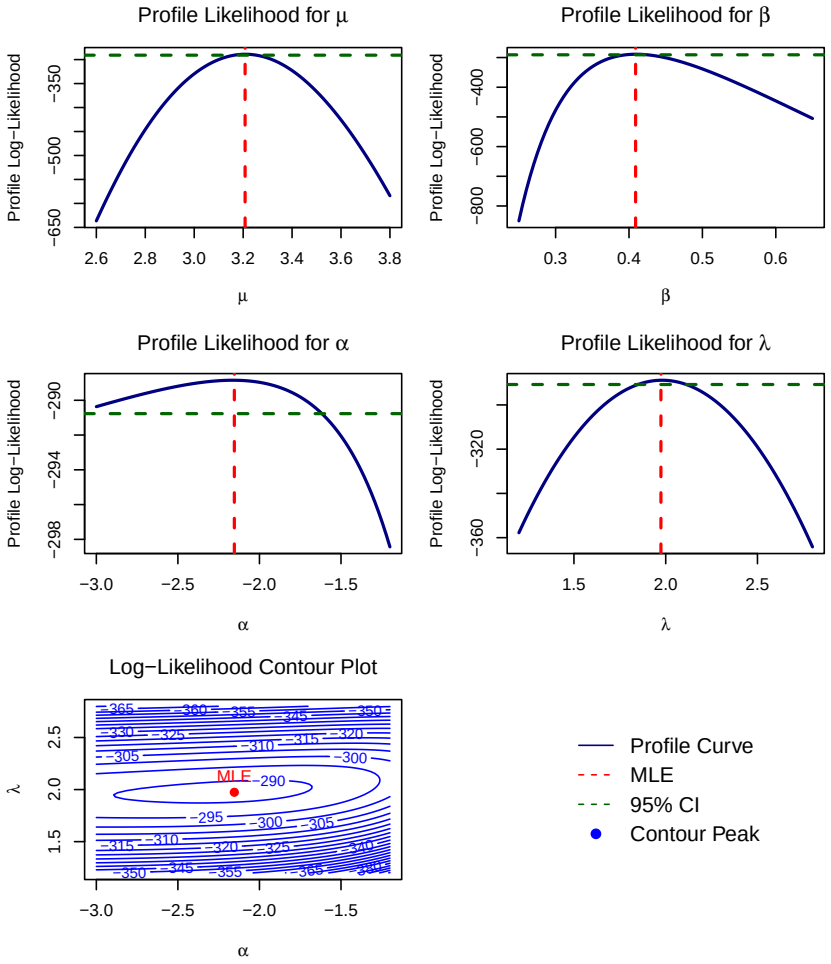

Figure 8. Profile log-likelihood plots for the parameters, along with the contour plot of the joint log-likelihood surface for (α, λ) for dataset I.

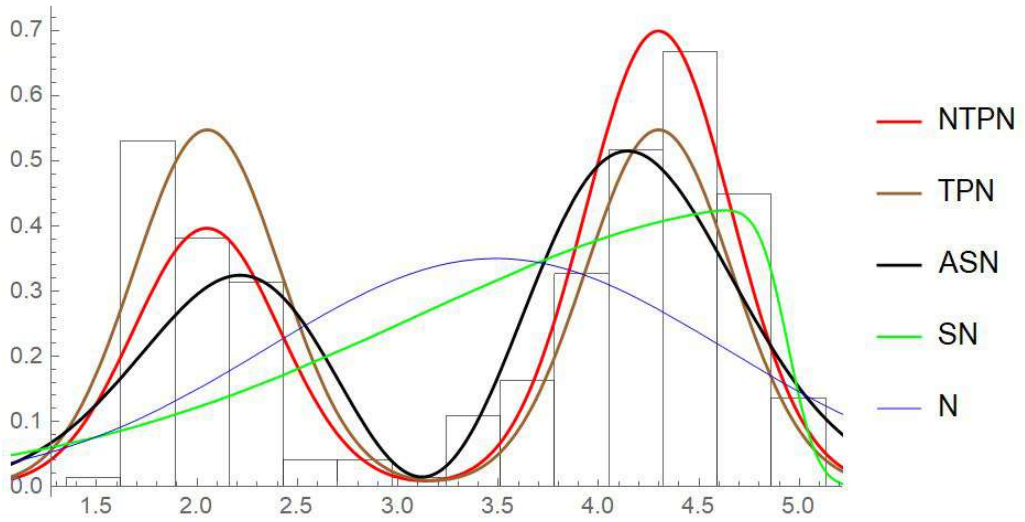

Figure 9. Visualizations illustrating observed versus expected density curves for dataset I.

6.2. Dataset II: Fatigue fracture data

This analysis uses the data consisting of the life of fatigue fracture of Kevlar 373/epoxy (sample size of 76) at fixed pressure until all had failed. The same data was previously used by [37] during his study. The various non-parametric graphs of the data are represented in Figure 10. The MLEs of the fitted models are shown in Table 9, together with the confidence intervals, log-likelihood, AIC, and BIC values. Meanwhile, Figure 11 presents the profile log-likelihood plots for the parameters μ, β, α, and λ of the $NTPN(\mu,\beta,\alpha,\lambda)$ distribution, together with the contour plot of the joint log-likelihood surface for (α,λ). Additionally, Figure 12 illustrates the performance and behavior of the models under consideration. Each curve achieves its maximum at the respective MLE, indicated by the red dashed line. The smooth and concave shapes of these curves confirm the regularity and unimodality of the likelihood surface, implying that the MLEs are well-defined and stable. The contour plot at the bottom shows the joint behavior of the parameters α and λ, where the elliptical contours centered around the MLE point indicate a well-behaved log-likelihood surface with moderate correlation between the two parameters. Overall, the plots validate that the estimation process for the NTPN model is numerically stable and provides reliable parameter estimates. According to Table 9, the AIC and BIC values associated with the NTPN distribution are smaller than those of the competing distributions. Furthermore, Figure 12 demonstrates the adequacy of the NTPN distribution in fitting the observed data. Accordingly, the NTPN distribution provides the best fit for the dataset under consideration.

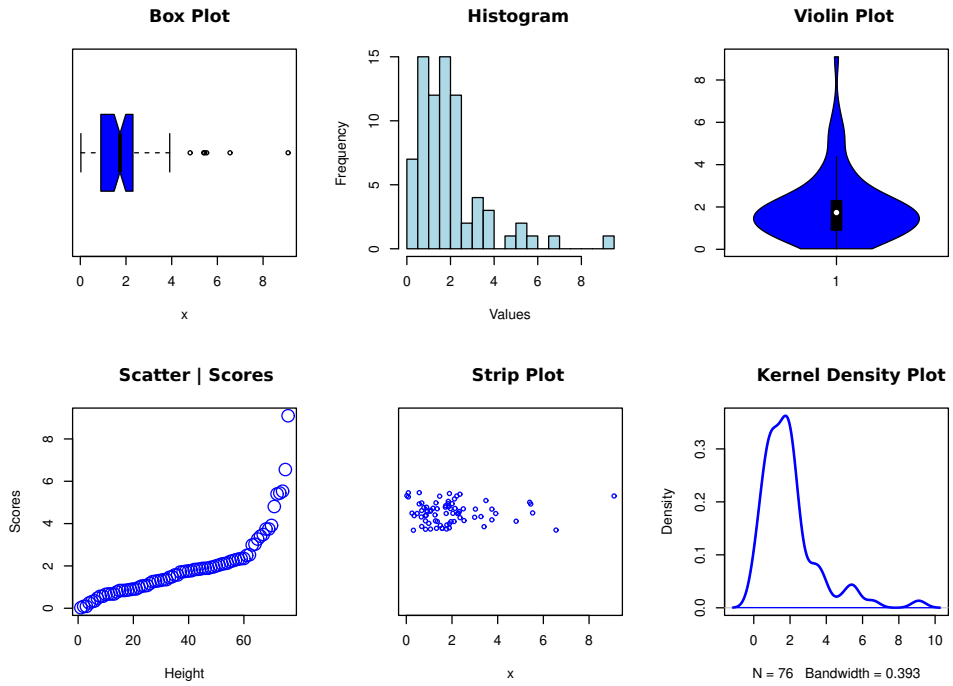

Figure 10. Nonparametric visualization plots for dataset II.

Table 9. Summary of model fit measures for dataset II.

Distribution	α	λ	μ	β	$\log L$	AIC	BIC
N	—	—	1.959	1.563	-141.81	287.62	292.28
	—	—	(1.607, 2.310)	(1.315, 1.812)			
ASN	1.518	—	3.004	1.306	-130.25	266.50	273.49
	(0.931, 2.106)	—	(2.622 , 3.386)	(1.110, 1.503)			
SN	—	1.760	0.839	1.827	-134.66	275.32	282.31
	—	(1.214, 2.306)	(0.512, 1.166)	(1.601, 2.053)			
TPN	—	0.001	1.929	1.564	-141.81	289.62	296.61
	—	(-0.318, 0.320)	(1.607, 2.311)	(1.290, 1.836)			
NTPN	0.622	1.796	3.663	0.959	**-127.96**	**263.92**	**273.24**
	(0.189, 1.055)	(0.955, 2.638)	(2.946, 4.380)	(0.802, 1.115)			

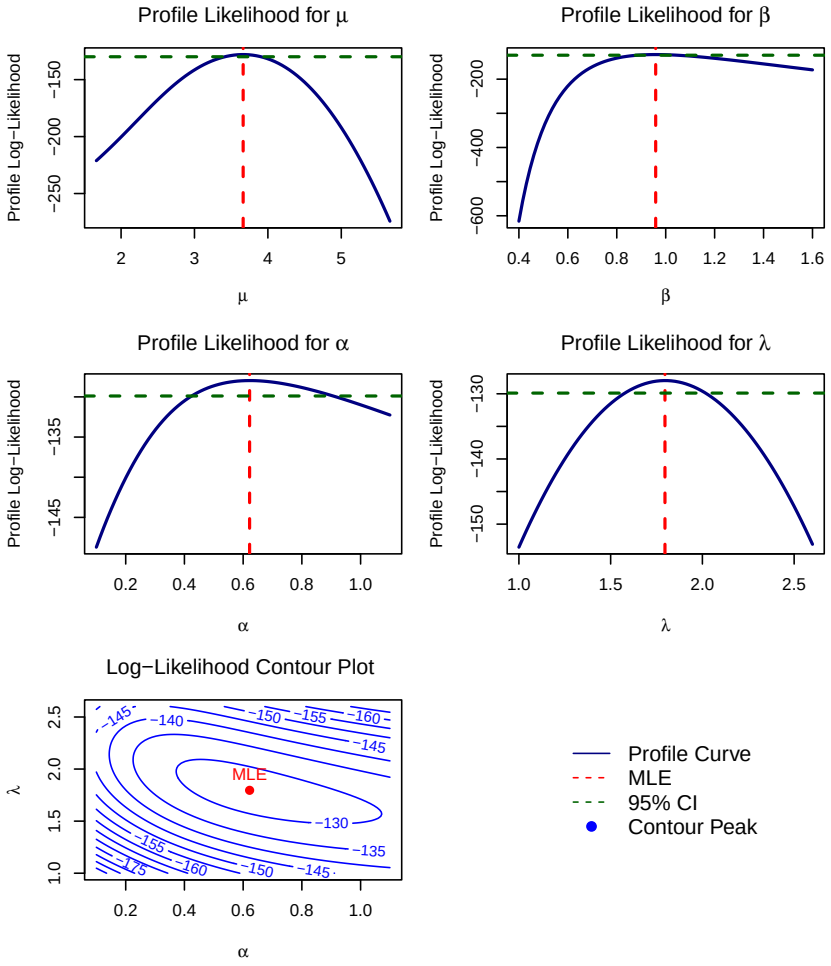

Figure 11. Profile log-likelihood plots for the parameters, along with the contour plot of the joint log-likelihood surface for (α, λ) for dataset II.

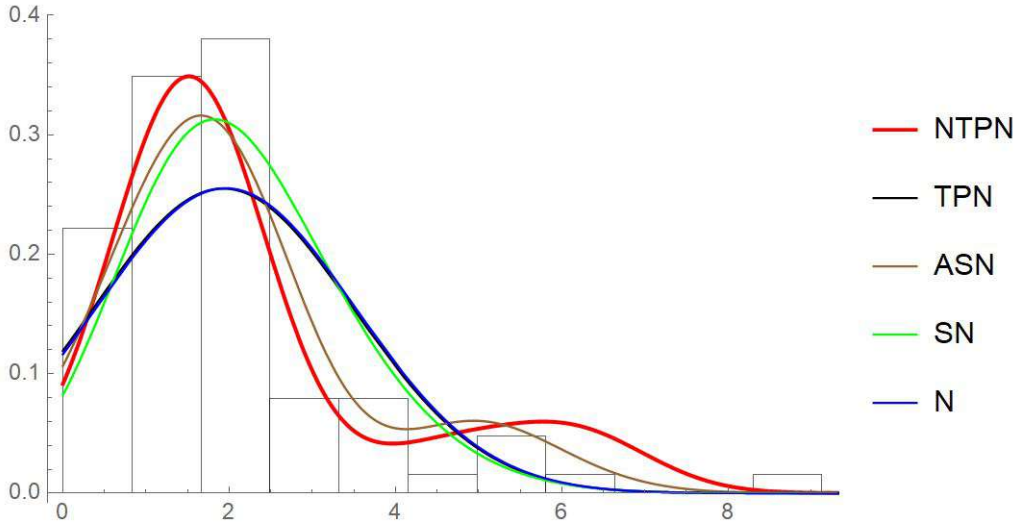

Figure 12. Visualizations illustrating observed versus expected density curves for dataset II.

7. Testing of hypothesis

In this section, the likelihood ratio test (LRT) is employed to discriminate between the proposed NTPN distribution and its nested or related models such as the N, ASN, and TPN distributions. The general form of the LRT statistic is given by

$$-2\log(LR) = -2\left[\log L(\hat{\boldsymbol{\theta}}_0) - \log L(\hat{\boldsymbol{\theta}}_1)\right],$$

where $\hat{\boldsymbol{\theta}}_0$ and $\hat{\boldsymbol{\theta}}_1$ denote the maximum likelihood estimates under the null and alternative hypotheses, respectively. Under the null hypothesis H_0, the statistic $-2\log(LR)$ is asymptotically distributed as χ^2_r, where r is the difference in the number of parameters between the two models.

The following hypotheses are considered:

(i) $H_0 : \alpha = 0, \lambda = 0$ (N model) vs. $H_1 : \alpha \neq 0, \lambda \neq 0$ (NTPN model), $r = 2$.
(ii) $H_0 : \lambda = 0$ (ASN model) vs. $H_1 : \lambda \neq 0$ (NTPN model), $r = 1$.
(iii) $H_0 : \alpha = 0$ (TPN model) vs. $H_1 : \alpha \neq 0$ (NTPN model), $r = 1$.

The LRT statistic for each case is computed as

$$-2\log(LR) = -2\left[\log L(\hat{\boldsymbol{\theta}}_0) - \log L(\hat{\boldsymbol{\theta}}_1)\right].$$

The LRT statistics in Table 10 are computed using the log-likelihood values from Tables 8 and 9. From Table 10, it is evident that for Dataset I, the computed LRT statistics for all comparisons are greater than their corresponding χ^2 critical values at the 5% level. This provides strong evidence in favor of the NTPN model over the N, ASN, and TPN models. Hence, based on the likelihood ratio test, the proposed NTPN distribution provides a significantly better fit for both datasets compared to its nested alternatives.

Table 10. The LRT results for datasets I and II.

Hypothesis	$-2\log(LR)$		**d.f.**	**Critical Value (5%)**	
	Dataset I	Dataset II		Dataset I	Dataset II
H_0 : N vs H_1 : NTPN	268.00	27.70	2	5.991	5.991
H_0 : ASN vs H_1 : NTPN	53.08	4.58	1	3.841	3.841
H_0 : TPN vs H_1 : NTPN	21.26	27.70	1	3.841	3.841

8. Conclusions

The NTPN distribution, which is a bimodal variant of the standard TPN model, is introduced as a novel and adaptable probability model in this article. The N, ASN, and TPN distributions are only a few of the famous models that are included as special cases in the proposed distribution. Explicit formulations for raw and central moments up to the fourth order, as well as the model's CDF, MGF, and Rényi entropy, have been obtained. Theoretical examination shows that the NTPN distribution can simulate symmetric, skewed, and bimodal data structures, and it also displays a large range of shapes. In addition, it is appropriate for modeling both overdispersed and underdispersed data,

and it has been proven that the distribution can only have two modes, proving its bimodality. We used the greatest likelihood technique to estimate the NTPN distribution's parameters. To get reliable parameter estimates, numerical optimization techniques were used, namely the GenSA global optimization algorithm in R, because the likelihood equations do not allow closed-form solutions. In order to evaluate the estimators' asymptotic precision and approximate their standard errors, the observed Fisher information matrix was also generated. A simulation analysis was carried out using the MH method to assess the MLEs' small-sample performance. The results showed that as the sample size increases, both the bias and the MSE decrease, validating the estimators' consistency. In a practical application, the NTPN distribution outperformed other models using goodness-of-fit metrics including log-likelihood, AIC, and BIC when tested on two real datasets. The stability of the parameter values and the smoothness and unimodality of the log-likelihood surface were further demonstrated using profile likelihood plots. Based on the results of the likelihood ratio test, the NTPN model is clearly superior to its nested counterparts when it comes to representing bimodal real-world data. To summarize, the NTPN distribution provides a robust and flexible extension of the two-piece normal family that may capture many data characteristics. Its usefulness in the literature on bimodal and asymmetric distributions is enhanced by its tractability and interpretability. Investigating Bayesian estimation methods, expanding the model to multivariate or matrix-variate forms, and applying it to broader domains like reliability analysis, financial risk modeling, environmental studies, and biostatistics, all of which deal with skewed or multimodal data, are all possible avenues for future research.

Author contributions

Reda Elbarougy: Investigation, data curation, validation, visualization, resources, writing-review & editing; Jondeep Das: Conceptualization, data curation, formal analysis, software, investigation, methodology, software, writing-original draft, writing-review & editing; Partha Jyoti Hazarika: Conceptualization, investigation, software, methodology, project administration, supervision, resources, validation, writing-review & editing; Mohamed S. Eliwa: Formal analysis, investigation, methodology, data curation, software, writing-review & editing, project administration. All authors read and approved the final manuscript.

Use of Generative-AI tools declaration

The authors declare they have not used Artificial Intelligence (AI) tools in the creation of this article.

Acknowledgments

The researchers would like to thank the Deanship of Graduate Studies and Scientific Research at Qassim University for financial support (QU-APC-2026).

Conflict of interest

The authors declare that they have no conflicts of interest.

References

1. S. Yang, D. Meng, H. Wang, C. Yang, A novel learning function for adaptive surrogate-model-based reliability evaluation, *Philos. T. Roy. Soc. A*, **382** (2024), 20220395. https://doi.org/10.1098/rsta.2022.0395
2. S. Yang, D. Meng, H. Yang, B. Keshtegar, A. M. P. D. Jesus, S. P. Zhu, Adaptive Kriging-assisted enhanced sparrow search with augmented-Lagrangian first-order reliability method for highly efficient structural reliability analysis, *Reliab. Eng. Syst. Safe.*, **267** (2026), 111916. https://doi.org/10.1016/j.ress.2025.111916
3. A. Azzalini, A class of distributions which includes the normal ones, *Scand. J. Stat.*, **12** (1985), 171–178.
4. S. Nadarajah, G. Aryal, On the skew uniform distribution, *Random Operators Sto.*, **12** (2004), 319–330. https://doi.org/10.1515/1569397042722337
5. G. Aryal, S. Nadarajah, On the skew Laplace distribution, *J. Inform. Optim. Sci.*, **26** (2005), 205–217. https://doi.org/10.1080/02522667.2005.10699644
6. S. Nadarajah, The skew logistic distribution, *AStA-Adv. Stat. Anal.*, **93** (2009), 187–203. https://doi.org/10.1007/s10182-009-0105-6
7. P. Theodossiou, Financial data and the skewed generalized t distribution, *Manage. Sci.*, **44** (1998), 1650–1661. https://doi.org/10.1287/mnsc.44.12.1650
8. S. Chakraborty, P. J. Hazarika, M. M. Ali, A new skew logistic distribution and its properties, *Pak. J. Stat.*, **28** (2012), 513–524. https://doi.org/10.1016/j.future.2011.09.005
9. M. R. Mahmoud, H. H. El-Damrawy, H. S. Abdalla, A new class of skew normal distribution: Tanh-skew normal distribution and its properties, *Int. J. Sci. Res. Sci. Technol.*, **5** (2020), 31–44.
10. N. B. Rushforth, P. H. Bennett, A. G. Steinberg, T. A. Burch, M. Miller, Diabetes in the Pima Indians: evidence of bimodality in glucose tolerance distributions, *Diabetes*, **20** (1971), 756–765. https://doi.org/10.2337/diab.20.11.756
11. A. O. Marcinek, M. Tabaka, Bimodal gene expression in noncooperative regulatory systems, *P. Natl. Acad. Sci. USA*, **107** (2010), 22096–22101. https://doi.org/10.1073/pnas.1008965107
12. G. V. Duarte, A. Braga, D. L. Miquelluti, V. A. Ozaki, Modeling of soybean yield using symmetric, asymmetric and bimodal distributions: Implications for crop insurance, *J. Appl. Stat.*, **45** (2018), 1920–1937. https://doi.org/10.1080/02664763.2017.1406902
13. R. S. Lima, A. Kucuk, C. C. Berndt, Bimodal distribution of mechanical properties on plasma sprayed nanostructured partially stabilized zirconia, *Mat. Sci. Eng. A*, **327** (2002), 224–232. https://doi.org/10.1016/S0921-5093(01)01530-1
14. J. McGee, J. A. Caverlee, Z. Cheng, *A geographic study of tie strength in social media*, In: Proceedings of the 20th ACM International Conference on Information and Knowledge Management, New York, USA, 2011, 2333–2336. https://doi.org/10.1145/2063576.2063959
15. H. Li, G. Fei, S. Wang, B. Liu, W. Shao, A. Mukherjee, et al., *Bimodal distribution and co-bursting in review spam detection*, In: Proceedings of the 26th International Conference on World Wide Web, 2017, 1063–1072. https://doi.org/10.1145/3038912.3052582

16. T. O. Lim, R. Bakri, Z. Morad, M. A. Hamid, Bimodality in blood glucose distribution: Is it universal? *Diabetes Care*, **25** (2002), 2212–2217. https://doi.org/10.2337/diacare.25.12.2212
17. D. E. Olivero, J. F. O. Pacheco, O. Venegas, H. Bolfarine, H. W. Gomez, On properties of the bimodal skew-normal distribution and an application, *Mathematics*, **8** (2020), 703. https://doi.org/10.3390/math8050703
18. J. Das, P. J. Hazarika, S. Chakraborty, D. Pathak, G. G. Hamedani, H. Karamikabir, A bimodal extension of the tanh skew normal distribution: Properties and applications, *Pak. J. Stat. Oper. Res.*, **20** (2024), 533–551.
19. D. E. Olivero, Alpha-skew-normal distribution, *Proyecciones (Antofagasta)*, **29** (2010), 224–240. http://dx.doi.org/10.4067/S0716-09172010000300006
20. P. J. Hazarika, S. Chakraborty, Alpha-skew-logistic distribution, *IOSR J. Math.*, **10** (2014), 36–46. https://doi.org/10.9790/5728-10463646
21. S. S. Harandi, M. H. Alamatsaz, Alpha–skew–Laplace distribution, *Stat. Probabil. Lett.*, **83** (2013), 774–782. https://doi.org/10.1016/j.spl.2012.11.024
22. M. Sharafi, Z. Sajjadnia, J. Behboodian, A new generalization of alpha-skew-normal distribution, *Commun. Stat.-Theor. M.*, **46** (2017), 6098–6111. https://doi.org/10.1080/03610926.2015.1117639
23. J. Das, P. J. Hazarika, D. Pathak, P. Sulewski, On a generalized Alpha skew Laplace distribution: Properties and applications, *Aust. J. Stat.*, **54** (2025), 125–150. https://doi.org/10.17713/ajs.v54i2.2025
24. P. J. Hazarika, S. Shah, S. Chakraborty, The Balakrishnan-alpha-skew-normal distribution: Properties and applications, *arXiv Preprint*, 2019. https://doi.org/10.48550/arXiv.1906.07424
25. S. Shah, S. Chakraborty, P. J. Hazarika, The Balakrishnan Alpha skew logistic distribution: Properties and applications, *Int. J. Appl. Math. Stat.*, **59** (2020), 76–92.
26. S. Shah, P. J. Hazarika, S. Chakraborty, A new Alpha skew Laplace distribution: Properties and its applications, *Int. J. Agric. Stat. Sci.*, **16** (2020), 1–10.
27. S. Shah, S. Chakraborty, P. J. Hazarika, M. M. Ali, The Log-Balakrishnan-alpha-skew-normal distribution and its applications, *Pak. J. Stat. Oper. Res.*, **16** (2020), 109–117.
28. E. G. Déniz, J. M. Sarabia, E. C. Ojeda, Bimodal normal distribution: Extensions and applications, *J. Comput. Appl. Math.*, **388** (2020), 113292. https://doi.org/10.1016/j.cam.2020.113292
29. E. G. Déniz, E. C. Ojeda, J. M. Sarabia, Bimodal and multimodal extensions of the normal and skew normal distributions, *REVSTAT-Stat. J.*, **23** (2023), 253–271. https://doi.org/10.57805/revstat.v23i2.563
30. A. Xu, J. Wang, D. Zhu, Z. Chen, Y. Wang, A robust Bayesian framework for degradation state identification in the presence of outliers, *Nav. Res. Log.*, 2025. https://doi.org/10.1002/nav.70033
31. A. Xu, W. Wang, Recursive Bayesian prediction of remaining useful life for gamma degradation process under conjugate priors, *Scand. J. Stat.*, 2025. https://doi.org/10.1111/sjos.70031
32. H. Salinas, H. Bakouch, N. Qarmalah, G. M. Flórez, A flexible class of two-piece normal distribution with a regression illustration to biaxial fatigue data, *Mathematics*, **11** (2023), 1271. https://doi.org/10.3390/math11051271

33. K. E. Muller, Computing the confluent hypergeometric function, M(a,b,x), *Numer. Math.*, **90** (2001), 179–196. https://doi.org/10.1007/s002110100285

34. K. T. Kumar, S. Remidi, A. D. Reddy, P. D. Reddy, R. S. Varun Kumar, J. Madhu, Numerical analysis of the radiative heat transfer and fluid flow between two cylinders using a high-order efficient Probabilists' Hermite polynomial based collocation method, *Numer. Heat Tr. B-Fund.*, **86** (2025), 1743–1762. https://doi.org/10.1080/10407790.2024.2320722

35. K. Peng, W. Chen, Maximum likelihood estimators and properties of the parameters of the Power Allamujia distribution under ranked set sampling, *J. Stat. Comput. Sim.*, **95** (2025), 3705–3727. https://doi.org/10.1080/00949655.2025.2542540

36. A. Azzalini, A. W. Bowman, A look at some data on the Old Faithful geyser, *Appl. Stat.*, **39** (1990), 357–365. https://doi.org/10.2307/2347385

37. A. Gul, A. J. Sandhu, M. Farooq, M. Adil, Y. Hassan, F. Khan, Half logistic-truncated exponential distribution: Characteristics and applications, *PLoS One*, **18** (2023), e0285992. https://doi.org/10.1371/journal.pone.0285992

AIMS Press